

# Kent Academic Repository

## Full text document (pdf)

### Citation for published version

Bokhovchuk, Fedir M and Bate, Neil and Kovalevskaya, Nadezhda V and Goult, Benjamin T and Spronk, Chris A E M and Vuister, Geerten W (2018) The Structural Basis of Calcium Dependent Inactivation of the Transient Receptor Potential Vanilloid 5 Channel. *Biochemistry* . ISSN 1520-4995.

### DOI

<https://doi.org/10.1021/acs.biochem.7b01287>

### Link to record in KAR

<http://kar.kent.ac.uk/66588/>

### Document Version

Author's Accepted Manuscript

#### Copyright & reuse

Content in the Kent Academic Repository is made available for research purposes. Unless otherwise stated all content is protected by copyright and in the absence of an open licence (eg Creative Commons), permissions for further reuse of content should be sought from the publisher, author or other copyright holder.

#### Versions of research

The version in the Kent Academic Repository may differ from the final published version.

Users are advised to check <http://kar.kent.ac.uk> for the status of the paper. **Users should always cite the published version of record.**

#### Enquiries

For any further enquiries regarding the licence status of this document, please contact:

[researchsupport@kent.ac.uk](mailto:researchsupport@kent.ac.uk)

If you believe this document infringes copyright then please contact the KAR admin team with the take-down information provided at <http://kar.kent.ac.uk/contact.html>

## The Structural Basis of Calcium Dependent Inactivation of the Transient Receptor Potential Vanilloid 5 Channel

Fedir M. Bokhovchuk, Neil Bate, Nadezhda V Kovalevskaya,  
Benjamin T. Goult, Chris A.E.M. Spronk, and Geerten W. Vuister

*Biochemistry*, **Just Accepted Manuscript** • DOI: 10.1021/acs.biochem.7b01287 • Publication Date (Web): 27 Mar 2018

Downloaded from <http://pubs.acs.org> on March 28, 2018

### Just Accepted

“Just Accepted” manuscripts have been peer-reviewed and accepted for publication. They are posted online prior to technical editing, formatting for publication and author proofing. The American Chemical Society provides “Just Accepted” as a service to the research community to expedite the dissemination of scientific material as soon as possible after acceptance. “Just Accepted” manuscripts appear in full in PDF format accompanied by an HTML abstract. “Just Accepted” manuscripts have been fully peer reviewed, but should not be considered the official version of record. They are citable by the Digital Object Identifier (DOI®). “Just Accepted” is an optional service offered to authors. Therefore, the “Just Accepted” Web site may not include all articles that will be published in the journal. After a manuscript is technically edited and formatted, it will be removed from the “Just Accepted” Web site and published as an ASAP article. Note that technical editing may introduce minor changes to the manuscript text and/or graphics which could affect content, and all legal disclaimers and ethical guidelines that apply to the journal pertain. ACS cannot be held responsible for errors or consequences arising from the use of information contained in these “Just Accepted” manuscripts.



1  
2  
3 **The Structural Basis of Calcium Dependent Inactivation of the**  
4 **Transient Receptor Potential Vanilloid 5 Channel**  
5  
6  
7

8  
9 ***Fedir M. Bokhovchuk<sup>1</sup>, Neil Bate<sup>1</sup>, Nadezda V. Kovalevskaya<sup>1,#</sup>, Benjamin T.***  
10 ***Goult<sup>1,&</sup>, Chris A.E.M. Spronk<sup>1,2,‡</sup> & Geerten W. Vuister<sup>1,\*</sup>***  
11  
12

13  
14  
15 <sup>1</sup> Department of Molecular and Cell Biology, Leicester Institute of Structural and  
16 Chemical Biology, University of Leicester, Lancaster Road, Leicester LE1 9HN,  
17 United Kingdom.  
18

19  
20 <sup>2</sup> JSC Spronk, Vilnius, Lithuania.  
21  
22

23 **# Present address:**

24  
25 Repositive Ltd, Future Business Centre, King's Hedges Road, Cambridge CB4 2HY,  
26 United Kingdom  
27

28 **& Present address:**

29  
30 School of Biosciences, University of Kent, Canterbury, Kent, CT2 7NJ, United Kingdom  
31

32  
33 ‡ Chris Spronk passed away on February 28<sup>th</sup> 2018  
34

35 \* Corresponding author (gv29@leicester.ac.uk)  
36  
37  
38  
39  
40  
41  
42  
43  
44  
45  
46  
47  
48  
49  
50  
51  
52  
53  
54  
55  
56  
57  
58

## Abstract

The Transient Receptor Potential Vanilloid Channel subfamily member 5 (TRPV5) is a highly selective calcium ion channel predominately expressed in the kidney epithelium that plays an essential role in calcium reabsorption from renal infiltrate. In order to maintain  $\text{Ca}^{2+}$  homeostasis, TRPV5 possesses a tightly regulated negative feedback mechanism, where the ubiquitous  $\text{Ca}^{2+}$ -binding protein Calmodulin (CaM) directly binds to the intracellular TRPV5 C-terminus, thus regulating TRPV5. Here we report on the characterisation of the TRPV5 C-terminal CaM binding site and its interaction with CaM at an atomistic level. We have solved the *de novo* solution structure of the TRPV5 C-terminus in complex with a CaM mutant, creating conditions that mimic the cellular basal  $\text{Ca}^{2+}$  state. We demonstrate that under these conditions the TRPV5 C-terminus is exclusively bound to the CaM C-lobe only, while conferring conformational freedom to the CaM N-lobe. We also show that at elevated calcium levels, additional interactions between the TRPV5 C-terminus and CaM N-lobe occur, resulting in formation of a tight 1:1 complex, effectively making the N-lobe the calcium sensor. Together, these data are consistent with, and support the novel model for  $\text{Ca}^{2+}$ /CaM-dependent inactivation of TRPV channels as proposed by Bate et al. (Biochemistry, 2018, in press).

### keywords

TRPV5 / calcium channel / NMR / structure / dynamics / calmodulin

## Introduction

The Transient Receptor Potential Vanilloid subfamily member 5 (TRPV5)\* is a highly-selective epithelial  $\text{Ca}^{2+}$  ion channel, predominately expressed in the apical epithelial membrane at the distal convoluted and connecting tubule of the kidney<sup>1</sup>. In the human kidney, approximately 95–98% of filtered  $\text{Ca}^{2+}$  is reabsorbed along renal tubules<sup>2</sup>. TRPV5 constitutes the apical entry gate for the transcellular reabsorption of  $\text{Ca}^{2+}$  along the tubule and thus plays a central role in reabsorption of  $\text{Ca}^{2+}$ . Gene knock-out studies showed that the ablation of TRPV5 results in a dramatic reduction of renal  $\text{Ca}^{2+}$  intake which concomitantly induces a compensatory hyperabsorption of dietary  $\text{Ca}^{2+}$  and bone abnormalities<sup>3</sup>. As TRPV5 is essential for the total body  $\text{Ca}^{2+}$ -homeostasis, its activity at the membrane is tightly regulated at the expression<sup>4</sup>, trafficking<sup>1,5</sup> and the level of turnover<sup>6</sup>.

When present at the plasma membrane under physiological levels of the membrane potential TRPV5 is constitutively open, resulting in a gradient-driven  $\text{Ca}^{2+}$  transport into the cell<sup>7</sup>. In order to be protected from the toxic influx of extracellular  $\text{Ca}^{2+}$ , electrophysiology studies demonstrated that TRPV5 employs a fast negative feedback gating mechanism, inactivating the channel upon elevated local intracellular  $\text{Ca}^{2+}$  concentration<sup>8</sup>. Several proteins that directly interact with TRPV5 intra-cellularly have been identified, including ones that also can bind  $\text{Ca}^{2+}$ . Examples of these are Calbindin-D28K<sup>9</sup>, S100A10<sup>1</sup>, 80-KH<sup>10</sup> and Calmodulin (CaM)<sup>8,11-13</sup>, where the latter was identified as a crucial factor in the  $\text{Ca}^{2+}$ -dependent inactivation of TRPV5.

Calmodulin is a highly conserved, ubiquitous  $\text{Ca}^{2+}$ - binding protein, essential as an intracellular  $\text{Ca}^{2+}$  sensor and regulator of the activity of many ion-channels in all eukaryotic cells. Functional CaM is comprised of 148 residues and has a dumbbell

---

\* **Abbreviations** CaM: Calmodulin; C-tail: C-terminal tail of the channel; CSP: chemical shift perturbation; HSQC: heteronuclear single-quantum correlation spectroscopy; ITC: isothermal titration calorimetry; NMR: nuclear magnetic resonance; N-tail: N-terminal tail of the channel; TRP: transient receptor potential; TRPV: transient receptor potential vanilloid; TRPV5<sup>655-725</sup>: transient receptor potential vanilloid 5 residues 655-725.

1  
2  
3 shaped structure formed by two domains, or lobes (subsequently denoted as the N-  
4 lobe and C-lobe), which are connected by a flexible linker region<sup>14,15</sup>.

5  
6  
7 For TRPV5, it was shown that the truncation of thirty of its C-terminal residues  
8 dramatically diminished Ca<sup>2+</sup>-dependent inactivation of the channel<sup>16</sup>. In silico  
9 prediction followed by subsequent biophysical characterization identified five  
10 putative CaM binding sites in the TRPV5 N- and C-terminal tails<sup>13</sup>. The most distal of  
11 these CaM binding regions at the C-terminus was shown crucial, as point mutants  
12 lacking CaM binding exhibited reduced Ca<sup>2+</sup>-dependent inactivation<sup>12</sup>. The closely  
13 related TRPV6 channel displayed a similar dependancy on CaM binding to the  
14 analogous region at its C-terminus<sup>17</sup>. Other members of the TRP family, i.e. for  
15 TRPC1<sup>18</sup>, TRPV1<sup>19</sup>, and TRPV4<sup>20</sup>, also showed a desensitization of the Ca<sup>2+</sup>-  
16 dependent negative feedback mechanism upon truncation of their C-terminal CaM  
17 binding sites. For TRPV2, CaM was shown to directly bind the intracellular C-  
18 terminus<sup>21</sup>. Taken together, these studies indicate that for TRPV5, binding of CaM to  
19 the C-terminal binding site is essential for the fast Ca<sup>2+</sup>-dependent inactivation of  
20 the channel. However, the molecular mechanism(s) by which CaM interacts with the  
21 TRPV5 terminus and exerts its inactivating mechanism remains unclear.

22  
23  
24 Atomic resolution structures of the N-terminal and membrane-spanning parts  
25 of the TRPV1<sup>22</sup>, TRPV2<sup>23</sup>, TRPV5<sup>24</sup> and TRPV6<sup>25,26</sup> channels have confirmed the  
26 predicted tetrameric assembly of the TRPV channels in analogy of the potassium  
27 and calcium ion channels. The structures have yielded invaluable knowledge on the  
28 ion-binding sites, pore structure, the location of the N-terminal Ankyrin repeat  
29 domains and the rearrangements of the membrane-spanning moieties leading to  
30 channel closure. However, in all structures the C-terminal parts of the channels  
31 were either omitted from the expression vectors or no data was obtained. Thus, the  
32 calcium-dependent regulation by CaM remains enigmatic.

33  
34  
35 Recently, Bate et al.<sup>27</sup> proposed a novel three-step regulatory model for TRPV6  
36 inactivation by CaM. According to this model, at basal intracellular Ca<sup>2+</sup> levels the  
37 TRPV6 C-terminus could be constitutively bound to the CaM C-lobe. Upon elevated  
38 Ca<sup>2+</sup>, additional interactions between the TRPV6 C-terminus and CaM N-lobe occur,  
39 which leads to a CaM-TRPV6 complex in which CaM bridges two TRPV6 channel C-  
40  
41  
42  
43  
44  
45  
46  
47  
48  
49  
50  
51  
52  
53  
54  
55  
56  
57  
58

1  
2  
3 termini, resulting in the formation of the inactivated form of the channel.  
4  
5 Considering the high level of homology between TRPV5 and TRPV6, as well as the  
6  
7 similar topology of their C-terminal CaM binding sites, it can be argued that both  
8  
9 channels share similar modes of Ca<sup>2+</sup>-dependent regulation.

10 The aim of the present work is to establish the structural organization of the  
11  
12 CaM:TRPV5 complex at different Ca<sup>2+</sup> conditions and thus, to suggest a mechanistic  
13  
14 basis for the Ca<sup>2+</sup>-dependent channel inactivation. Therefore, we employed high-  
15  
16 resolution analytical gel filtration and NMR spectroscopy on various CaM-TRPV5  
17  
18 complexes to study the interaction at an atomistic level. We present the solution  
19  
20 structure of the CaM-TRPV5 complex in a low-calcium mimicking state and establish  
21  
22 how its dynamic behaviour relates to the high-calcium state leading to channel  
23  
24 inactivation.  
25

## 26 **Materials and Methods**

### 27 **Protein expression and purification**

28  
29  
30  
31 The C-terminal fragment TRPV5<sup>655-725</sup> was amplified by PCR and inserted into  
32  
33 the *E.coli* expression vector, pLEICS-46, which contains a 58-amino acid GB1  
34  
35 solubility tag and a His<sub>6</sub> affinity tag followed by a TEV cleavage site (Protex,  
36  
37 University of Leicester). CaM wild-type and CaM mutants defunct in calcium binding  
38  
39 to the N-lobe, C-lobe or both lobes, denoted as CaM<sub>12</sub>, CaM<sub>34</sub> and CaM<sub>1234</sub>  
40  
41 respectively<sup>28</sup>, were amplified by PCR and inserted into the *E.coli* expression vector,  
42  
43 pLEICS-01, which contains a His<sub>6</sub> affinity tag followed by a TEV cleavage site  
44  
45 (Protex, University of Leicester). All constructs were sequence verified. Plasmids  
46  
47 were expressed in *E.coli* BL21 Star (DE3) (Life Technologies, USA) grown in either  
48  
49 LB, or in 2M9 minimal media for the production of unlabelled, <sup>15</sup>N- or <sup>15</sup>N/<sup>13</sup>C-  
50  
51 labelled samples for NMR experiments. Cultures were grown at 37 °C to an OD<sub>600</sub> of  
52  
53 approximately 0.8 and induced with IPTG to a final concentration of 200 μM for CaM  
54  
55 and 40 μM for TRPV5, and incubated overnight at 18 °C. Cells were harvested and  
56  
57 the pellet resuspended in buffer containing 20 mM Tris-Cl pH 8.0, 50 mM imidazole,  
58  
59 500 mM NaCl and protease inhibitors (Protease Inhibitor Cocktail Set III,  
60

1  
2  
3 Calbiochem). Cell disruption was achieved via sonication and the cleared lysate  
4 applied to a HisTrap™ HP column (GE Healthcare). Recombinant proteins were  
5 eluted with an imidazole gradient of 0.05-0.5 M, dialysed into 20 mM Tris-Cl pH 8.0,  
6 50 mM NaCl, 1 mM DTT and concomitantly cleaved with TEV protease to remove N-  
7 terminal tags; GB1-His<sub>6</sub>- (pLEICS-46) and His<sub>6</sub>- (pLEICS-01). Cleaved recombinant  
8 proteins were further purified via anion exchange using a HiTrap™ Q HP column  
9 (GE Healthcare) and eluted with a NaCl gradient of 0.05-1 M. Recombinant proteins  
10 were analysed by 16% SDS-PAGE and stained using Coomassie brilliant blue R-250.  
11 Protein concentrations were determined from the UV absorbance at 280 nm,  $A_{280}$   
12 (Eppendorf BioPhotometer plus) using the extinction coefficients  $\epsilon(\text{CaM}_{\text{WT}/12})=2980$   
13  $\text{M}^{-1}\text{cm}^{-1}$ ,  $\epsilon(\text{TRPV5}^{655-725})=5500 \text{ M}^{-1}\text{cm}^{-1}$  as determined by the ProtParam Tool  
14 (<http://web.expasy.org/protparam>).  
15  
16  
17  
18  
19  
20  
21  
22  
23  
24

### 25 **Analytical gel filtration**

26  
27 Recombinant CaM and TRPV6 proteins were dialysed into gel filtration buffer  
28 (20 mM Tris-Cl pH 8.0, 150 mM NaCl and 2 mM DTT). Complexes were formed in the  
29 presence of 10 mM  $\text{Ca}^{2+}$  at room temperature for 30 minutes. Analytical gel filtration  
30 chromatography was carried out using a Superdex75 (10/300) column (GE  
31 Healthcare) pre-equilibrated and then run in gel filtration buffer.  
32  
33  
34  
35  
36  
37  
38

### 39 **NMR spectroscopy and sample preparation**

40 The CaM:peptide complex under a low  $[\text{Ca}^{2+}]$  (100-300 nM) was achieved by  
41 repeated dialysis: first against 20 mM Tris-Cl pH 7.4, 2 mM EGTA pH 8.0, and  
42 subsequently against 20 mM Tris-Cl pH 7.4. The effective  $[\text{Ca}^{2+}]$  was estimated on  
43 the basis of ionic composition listed by the manufacturer of our chemicals used for  
44 preparation of the buffer. All other CaM:TRPV5 complexes were prepared using the  
45 following steps: FPLC Q-column CaM and TRPV5 protein fractions were separately  
46 dialyzed against NMR buffer (20 mM Tris pH 7.4, 50 mM KCl, 10 mM  $\text{CaCl}_2$ ); the  
47 concentration was determined and components mixed at the required ratio; protein  
48 complexes were concentrated using a 3.5 kDa molecular weight cut-off centricon  
49  
50  
51  
52  
53  
54  
55  
56  
57  
58



1  
2  
3 filter (Millipore, USA). CaM<sub>E</sub> and the CaM<sub>E</sub>:TRPV5 co-expression complex were  
4 dialyzed against (pH 7.4, 60 mM KCl, 20 mM Tris). All NMR samples contained 5%  
5 v/v D<sub>2</sub>O.  
6  
7

### 10 **NMR spectra recording, processing and assignment**

11 The NMR spectra were recorded at 35 °C on Bruker 500 MHz AVI, 600 MHz  
12 AVIII, 600 MHz AVIII HD, or 800 MHz AVII spectrometers; the 600 MHz and 800  
13 MHz spectrometers were equipped with CryoProbes. NMR data processing and  
14 analysis were performed using the NMRPipe<sup>29</sup>, TOPSPIN v3.1 and CcpNmr  
15 Analysis<sup>30</sup> and AnalysisAssign<sup>31</sup> software. Non-uniformly sampled 3D and 4D  
16 spectra were reconstructed using the istHMS software<sup>32</sup>.  
17  
18

19 The binding of TRPV5 to CaM was monitored by 2D <sup>15</sup>N-<sup>1</sup>H-HSQC experiments.  
20 The previously published assignment of CaM (BMRB entry 547) was used as a  
21 starting point. For the near complete assignment of the backbone atoms of the  
22 different CaM:TRPV5 complexes, the following series of heteronuclear triple-  
23 resonance experiments were performed: 3D HNCA, HNCACB, HN(CO)CA,  
24 CBCA(CO)NH, HNCOC for the unbound <sup>13</sup>C-<sup>15</sup>N-CaM<sub>WT</sub> and <sup>13</sup>C-<sup>15</sup>N-CaM<sub>12</sub> and the  
25 following complexes (Supplementary Tables 1.1 and 1.2): <sup>13</sup>C-<sup>15</sup>N-CaM<sub>WT</sub>:TRPV5<sup>655-725</sup>-  
26 <sup>725</sup> (1:1), <sup>13</sup>C-<sup>15</sup>N-CaM<sub>WT</sub>:TRPV5<sup>655-725</sup> (1:2), <sup>15</sup>N-CaM<sub>WT</sub>:<sup>13</sup>C-<sup>15</sup>N-TRPV5<sup>655-725</sup> (1:1)  
27 and CaM<sub>12</sub>:<sup>13</sup>C-<sup>15</sup>N-TRPV5<sup>655-725</sup> (1:1). CaM chemical shifts differences resulting from  
28 binding were calculated for each individual backbone amide peak as  
29  
30  
31  
32  
33  
34  
35  
36  
37  
38  
39  
40

$$41 \quad \Delta\delta = \sqrt{(\Delta\delta_H)^2 + 0.15(\Delta\delta_N)^2} \quad (1)$$

42 where  $\Delta\delta_H$  and  $\Delta\delta_N$  are the chemical shift differences for <sup>1</sup>H and <sup>15</sup>N, respectively. In  
43 order to assign peaks from disordered region of the TRPV5 moiety of the complex,  
44 direct <sup>13</sup>C-detected experiments were employed<sup>33,34</sup>. Side-chain atoms were  
45 assigned by comparison of the strips of the 3D <sup>13</sup>C (H)CCH/H(C)CH-TOCSY<sup>35</sup> spectra,  
46 recorded on Bruker 600 MHz AVIII and 600 MHz AVIII HD spectrometers, and a  
47 constant time <sup>13</sup>C-HSQC spectrum. Two-dimensional CBHD/CB(HD)HE<sup>36</sup> spectra  
48  
49  
50  
51  
52  
53  
54  
55  
56  
57  
58

1  
2  
3 were used in order to unambiguously link  $\beta$ -carbon and aromatic protons of the  
4 CaM<sub>12</sub> aromatic residues.  
5  
6  
7

### 8 **<sup>15</sup>N-relaxation experiments**

9  
10 <sup>15</sup>N-T<sub>1</sub>, <sup>15</sup>N-T<sub>2</sub> and heteronuclear <sup>1</sup>H-<sup>15</sup>N-NOE data were collected at 35 °C at  
11 14.1 T (and 18.8 T as a control) using standard pulse sequences. Eight data points  
12 were measured for both T<sub>1</sub> and T<sub>2</sub>, with the range of delays between 8 to 1120 ms  
13 and 4.6 to 110.4 ms, respectively, in randomized order. In the heteronuclear NOE  
14 experiment, a relaxation delay of 2.9 s was used prior to each scan. Residues with  
15 peaks overlapping in the <sup>15</sup>N-HSQC spectra were excluded from the relaxation  
16 analysis. T<sub>1</sub> and T<sub>2</sub> data were fitted using the nLinLS and expFit modules of the  
17 NMRPipe software package<sup>29</sup>. Intensities were subsequently fitted to an exponent  
18 using the modelXY module in NMRPipe and rates obtained. Errors of the rates were  
19 estimated using Monte-Carlo simulations from the errors of the measured peak  
20 intensities. The local rotational correlation time, ( $\tau_c$ ), for each individual amide  
21 group was calculated from the T<sub>2</sub>/T<sub>1</sub> ratio according to Fushman et al.<sup>37</sup>.  
22  
23  
24  
25  
26  
27  
28  
29  
30  
31  
32

### 33 **Structure calculation and validation**

34  
35 NMR NOESY spectra for aliphatic and aromatic regions were recorded at 35 °C  
36 on a Bruker 800 MHz AVII spectrometer. The NOE-mixing time was set to 80 ms in  
37 all NOESY experiments. The structures were calculated, refined and validated using  
38 the CcpNMR Analysis pipeline using CYANA3.97<sup>38</sup> as described by Skinner et al.<sup>39</sup>.  
39 For the structure determination, the NOESY cross peaks were automatically picked  
40 and integrated by CcpNMR Analysis and then manually checked for artefacts and  
41 genuinely missed peaks by comparison of the <sup>13</sup>C-NOESY strips with the  
42 corresponding strip of the <sup>13</sup>C-TOCSY spectra. The complex was treated as a single  
43 chain in CYANA3.97, with CaM<sub>12</sub> and TRPV5<sup>655-725</sup> sequences connected by the  
44 lengthy sequence of linker residues. Also, two Ca<sup>2+</sup> ions were added to the sequence  
45 and linked to the side-chain carboxylates or carbonyls of the Asp and Glu residues  
46 93, 95, 97, 104 and 129, 131, 133, 140 from the C-lobe EF-domains 3 and 4,  
47 respectively. The input data for CYANA consisted of the table of chemical shifts,  
48  
49  
50  
51  
52  
53  
54  
55  
56  
57  
58

1  
2  
3 unassigned peaks (positions and volumes) of the NOESY spectra, backbone dihedral  
4 restraints for both moieties of the complex, as predicted from the chemical shifts  
5 values by the programs TALOS+<sup>40</sup> and DANGLE<sup>41</sup>, the list of unambiguous inter-  
6 chain distance restraints, which was obtained by manual assignment of the  
7 reciprocal CaM<sub>12</sub> and TRPV5<sup>655-725</sup> NOESY peaks and set to 5.5 Å, and the list of  
8 lower- and upper limit distance restraints for the Ca<sup>2+</sup> ion coordinate bonds, which  
9 were set to 2 Å and 3 Å, respectively.

10  
11  
12 The NOESY peaks lists were automatically assigned during seven cycles of  
13 automated assignment and structure calculation using CYANA/CANDID protocol. In  
14 each cycle, 120 structures were generated and energy minimized using 15,000  
15 simulations steps. The NOESY spectra parameters were calibrated in the first cycle.  
16 Quality of the calculated structural NMR ensemble was analysed and validated with  
17 the CING suite available at the iCing webserver (<https://nmr.le.ac.uk>)<sup>42</sup>. The 20  
18 lowest energy conformers were subsequently subjected to a final round of  
19 refinement using YASARA<sup>43</sup> in two stages. In the first stage, the CYANA structures  
20 were subjected to refinement in explicit solvent using a regular flat bottom  
21 harmonic well restraints potential with the upper limits from the CYANA consensus  
22 restraints. The resulting refined ensemble was then used in combination with the  
23 peak volumes to calibrate Log Normal target distances according to the method,  
24 suggested by Bardiaux et al.<sup>44</sup>. In the second stage these target distances were used  
25 for further explicit solvent refinement of the structures using log-normal  
26 potentials<sup>45</sup>. A table of structure quality metrics, based on the iCing report was  
27 assembled as recommended by the wwPDB NMR Validation Task Force<sup>46</sup>.

## 43 44 45 **Results**

46  
47  
48 Previously, we probed the minimal TRPV5 binding sites using short  
49 peptides<sup>13</sup>. Here, we employed the longest soluble TRPV5 C-terminal construct  
50 residues 655-725, denoted as TRPV5<sup>655-725</sup><sup>47</sup>, to examine its interactions with CaM.  
51 Comparison of the <sup>15</sup>N-HSQC spectra of the CaM<sub>wt</sub> complex of the longer 655-725  
52 construct used in this study with the complex of the short peptide used previously,  
53  
54  
55  
56  
57  
58

1  
2  
3 shows notable differences (Fig. S1A), suggesting additional effects caused by  
4 residues outside the previously postulated binding region. Also, for the paralogue  
5 TRPV6 it was established that the flanking residues were crucial in CaM-dependent  
6 inactivation<sup>27</sup>. Consequently, this renders our current, longer construct a better  
7 model for studying the CaM-TRPV5 interaction.  
8  
9

10  
11 We first set out to establish the nature of the CaM-TRPV5 interaction under  
12 low [Ca<sup>2+</sup>]. Both N- and C- CaM lobes contain two EF hands (helix-loop-helix motifs)  
13 that together can bind up to four Ca<sup>2+</sup> ions per molecule of CaM<sup>15</sup>. Despite the high  
14 sequence similarity of the two globular domains, it was shown *in vitro* that Ca<sup>2+</sup> ions  
15 binds to the CaM C-lobe with a positive cooperativity and individual macroscopic  
16 equilibrium dissociation constants (K<sub>d</sub>) between 25 and 200 nM, whereas  
17 approximately 6 times lower affinity for the N-lobe was reported<sup>48</sup>. Consequently,  
18 given that the resting cytosolic concentrations of free Ca<sup>2+</sup> in the epithelial cells is  
19 about 100 nM<sup>49</sup>, the CaM C-lobe is expected to be at least partially Ca<sup>2+</sup> loaded at  
20 basal conditions, whereas the N-lobe is fully Ca<sup>2+</sup>-loaded only under conditions of  
21 significant calcium influx. In order to investigate the interactions of TRPV5 and CaM  
22 under representative basal cellular conditions, we purified <sup>15</sup>N-CaM<sub>WT</sub> from *E.coli*  
23 where neither exogenous Ca<sup>2+</sup>, nor Ca<sup>2+</sup>-chelating agents were added during protein  
24 purification (denoted as CaM<sub>E</sub>). The <sup>15</sup>N-HSQC spectrum of CaM<sub>E</sub> reveals that it  
25 exists as a heterogeneous mixture under these conditions, that can be readily  
26 resolved by the subsequent addition of excess Ca<sup>2+</sup> (Figs S2A-C). In accordance with  
27 the ~6 fold higher affinity of the CaM C-lobe for Ca<sup>2+</sup> compared to the N-lobe, the  
28 spectra show that Ca<sup>2+</sup> binds initially to the CaM C-lobe predominantly, followed by  
29 binding of Ca<sup>2+</sup> into the N-lobe. Moreover, only 2.5 equivalents of Ca<sup>2+</sup> are required  
30 to convert one CaM<sub>E</sub> to a fully Ca<sup>2+</sup>-loaded state (Fig. S2C, compare with Fig. S2B),  
31 showing that each CaM<sub>E</sub> moiety is on-average loaded with ~1 Ca<sup>2+</sup> ion. Since the  
32 intracellular concentration of free Ca<sup>2+</sup> in *E.coli* is ~90 nM<sup>50</sup>, which is approximately  
33 the same as determined for renal epithelial cells<sup>49</sup>, we believe CaM<sub>E</sub> to be a good  
34 representative of resting free intracellular CaM.  
35  
36  
37  
38  
39  
40  
41  
42  
43  
44  
45  
46  
47  
48  
49  
50  
51  
52  
53

54 Next, as a proxy for complex formation under cellular conditions we used a  
55 transcriptional fusion to co-express His<sub>6</sub>-CaM and a tag-less TRPV5<sup>655-725</sup> C-tail in  
56  
57

1  
2  
3 *E.coli*. We co-purified a  $^{15}\text{N}$ -CaM<sub>E</sub> /  $^{15}\text{N}$ -CaM<sub>E</sub> - $^{15}\text{N}$ -TRPV5<sup>655-725</sup> mixture using the  
4 His<sub>6</sub> tag attached to CaM, again without addition of exogenous Ca<sup>2+</sup> or Ca<sup>2+</sup>-chelating  
5 agents, and examined this sample response to increasing [Ca<sup>2+</sup>] using  $^{15}\text{N}$ -HSQC  
6 experiments (Fig. 1 and Figs S2D-H). The spectra showed that the sample comprised  
7 a heterogeneous mixture of both free CaM<sub>E</sub> and CaM<sub>E</sub> bound to TRPV5, which  
8 displayed a differential behaviour upon addition of exogenous Ca<sup>2+</sup> (Fig. 1A). We  
9 used the relative intensities of representative cross-peaks as a proxy for the  
10 presence and/or dynamic exchange of Ca<sup>2+</sup> in these different states. The signals  
11 from the CaM<sub>E</sub> C-lobe in complex with TRPV5<sup>655-725</sup> are unaffected by increasing  
12 [Ca<sup>2+</sup>] (Fig. 1B), indicating that the C-lobe has effectively sequestered Ca<sup>2+</sup> in both its  
13 Ca<sup>2+</sup>-binding sites. In contrast, the signals of free, i.e. non-complexed, CaM<sub>E</sub> C-lobe  
14 show a steady increase in intensity (Fig. 1C), with its maximum reached after the  
15 addition of 3 equivalents of Ca<sup>2+</sup>, similar to that previously seen for CaM<sub>E</sub> in  
16 isolation. Hence, the behaviour of CaM<sub>E</sub> under resting cellular [Ca<sup>2+</sup>] is very different  
17 depending on whether it is in complex with TRPV5<sup>655-725</sup>. In the absence of  
18 TRPV5<sup>655-725</sup>, CaM<sub>E</sub> exists in a mixture of calcium bound states; however, the  
19 presence of TRPV5<sup>655-725</sup> stabilises the fully Ca<sup>2+</sup>-loaded C-lobe. Therefore, we  
20 conclude that at basal conditions the tail of the TRPV5 channel can be bound to a  
21 fully Ca<sup>2+</sup>-loaded C-lobe.  
22  
23  
24  
25  
26  
27  
28  
29  
30  
31  
32  
33  
34  
35

36 To test our ability to reproduce these results under *in vitro* conditions we  
37 first generated CaM<sub>WT</sub>:TRPV5<sup>697-712</sup> complexes at fully-apo, basal and elevated  
38 intracellular Ca<sup>2+</sup> concentrations and recorded  $^{15}\text{N}$ -HSQC spectra (Figs 1D,E).  
39 Careful comparison of these spectra shows that under basal cytosolic Ca<sup>2+</sup>  
40 concentration, the CaM<sub>WT</sub> C-lobe again appears in a Ca<sup>2+</sup>-loaded and bound state,  
41 whereas the data are consistent with an N-lobe devoid of Ca<sup>2+</sup> or TRPV5 interaction.  
42  
43  
44  
45  
46  
47  
48  
49  
50  
51  
52  
53  
54  
55  
56  
57  
58  
59  
60

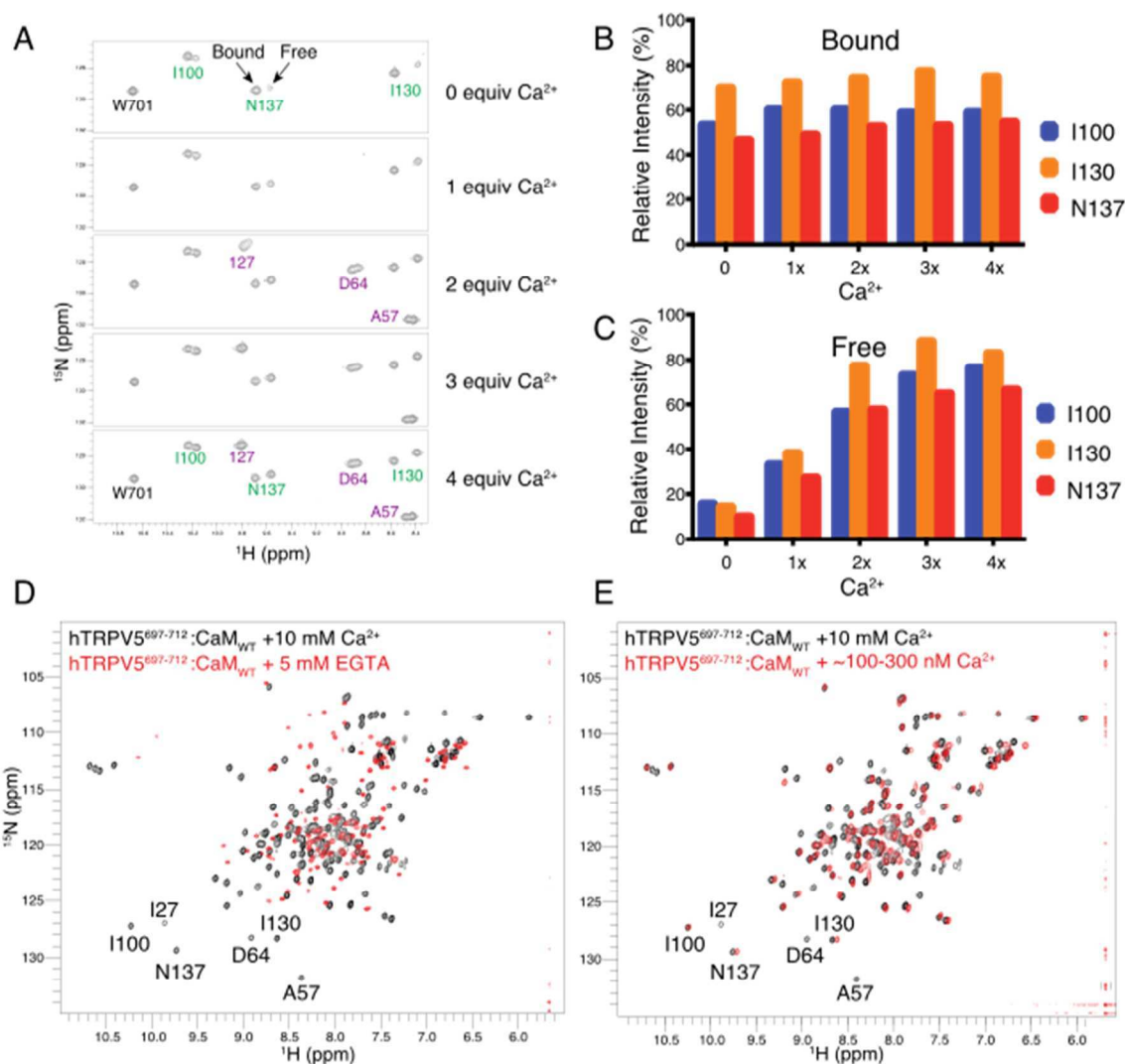


**Figure 1. Calmodulin is bound via its C-lobe to the TRPV5 C-tail under low  $\text{Ca}^{2+}$  conditions.**

(A) Small regions of the  $^{15}\text{N}$ - $^1\text{H}$ -HSQC spectra of  $^{15}\text{N}$ -labelled CaM and  $^{15}\text{N}$ -labeled TRPV5<sup>655-725</sup>, which were co-expressed in *E.coli* and purified in the absence of exogenous  $\text{Ca}^{2+}$ , at increasing  $\text{Ca}^{2+}$ -stoichiometries. Selected residues are indicated. Full spectra displayed in Figs S2(D-H); (B, C) Comparison of the relative peak intensities for different residues in (B) bound and (C) free states, derived from the spectra displayed in (A) using TRPV5 residue W701 as calibration reference; (D)  $^{15}\text{N}$ -HSQC spectra of  $\text{CaM}_{\text{WT}}$  in complex with 2x amount of TRPV5<sup>697-712</sup> upon addition of 10 mM  $\text{CaCl}_2$  (black) and 5mM EGTA (red); (E)  $^{15}\text{N}$ -HSQC spectra of  $\text{CaM}_{\text{WT}}$  in complex with 2x amount of TRPV5<sup>697-712</sup> upon addition of 10 mM  $\text{CaCl}_2$  (black) and with residual amounts of  $\text{Ca}^{2+}$  (no  $\text{Ca}^{2+}$  added during purification/sample preparation; see methods) (red).

1  
2  
3  
4  
5 In order to study the larger and more representative CaM:TRPV5<sup>655-725</sup>  
6 complex at low Ca<sup>2+</sup> concentration in a highly controlled and reproducible fashion,  
7 for NMR experiments we employed a previously described E32Q/E68Q N-lobe  
8 double mutant, denoted as CaM<sub>12</sub>, which prevents the N-lobe from binding Ca<sup>2+</sup>  
9 while retaining the full Ca<sup>2+</sup> binding capacity for the C-lobe<sup>28</sup>. First, binding of this N-  
10 lobe functional mutant to TRPV5<sup>655-725</sup> was studied by analytical gel-filtration at  
11 high-Ca<sup>2+</sup> conditions along with the CaM<sub>34</sub> and CaM<sub>1234</sub> mutants, where the Ca<sup>2+</sup>-  
12 binding sites are mutated in the C-lobe or in both lobes, respectively. Similar to the  
13 corresponding TRPV6 region<sup>27</sup>, the formation of the stable complex was observed by gel  
14 filtration only for CaM<sub>12</sub>:TRPV5<sup>655-725</sup> (Fig. S3A), whereas no evidence of interaction  
15 was found for CaM<sub>34</sub> (Fig. S3B) or CaM<sub>1234</sub> (Fig. S3C). Systematic comparisons of the  
16 NMR data collected for the CaM<sub>WT</sub>:TRPV5<sup>697-712</sup> complexes under various [Ca<sup>2+</sup>] and  
17 the CaM<sub>12</sub>:TRPV5<sup>655-72</sup> complex (cf. compare Fig. S1B and Fig. 1E) indicates the latter  
18 to be a valid model for the CaM:TRPV5 complex at the basal calcium state.  
19  
20  
21  
22  
23  
24  
25  
26  
27  
28  
29  
30  
31

### 32 ***CaM:TRPV5<sup>655-725</sup> interaction at different Ca<sup>2+</sup> conditions***

33  
34 To identify CaM amino acids involved in the interaction with TRPV5,  
35 changes in <sup>1</sup>H-<sup>15</sup>N cross-peak positions in response to varying concentrations of  
36 TRPV5 were monitored. 2D <sup>1</sup>H-<sup>15</sup>N HSQC spectra of <sup>15</sup>N-CaM<sub>12</sub> and <sup>15</sup>N-CaM<sub>wt</sub> in the  
37 ligand-free apo-state and upon addition of an equimolar, and 2-fold excess of  
38 unlabelled TRPV5<sup>655-725</sup> were collected, overlaid and analysed. This analysis  
39 revealed significant differences in patterns of the perturbations of the peaks of  
40 distinct N- and C-lobe amino acids upon binding (Figs 2A,B). In order to investigate  
41 this interaction for the whole CaM backbone, conventional heteronuclear multi-  
42 dimensional triple-resonance NMR methods were utilized to assign the <sup>1</sup>H, <sup>15</sup>N and  
43 <sup>13</sup>C backbone resonances of CaM<sub>wt</sub> and CaM<sub>12</sub> as 1:1 and 1:2 complexes with  
44 unlabelled TRPV5<sup>655-725</sup> along with apo-<sup>15</sup>N-CaM<sub>12</sub>. Overall, more than 95% of  
45 backbone resonances were unambiguously assigned for all complexes, excluding  
46 Prolines 43 and 66, and Ser 81 from the flexible linker connecting the CaM N- and C-  
47  
48  
49  
50  
51  
52  
53  
54  
55  
56  
57  
58  
59  
60

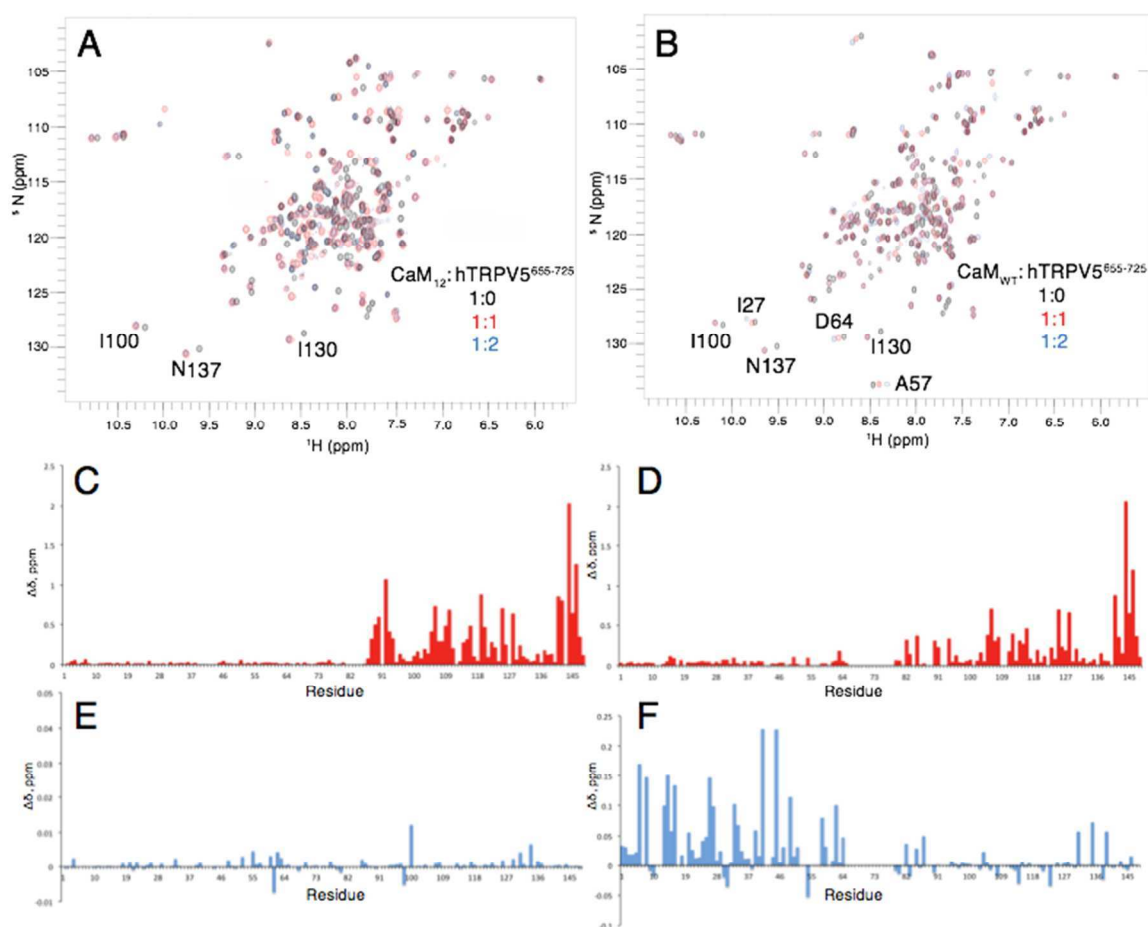


**Figure 2. NMR data of the CaM<sub>12</sub>:TRPV5<sup>655-725</sup> and CaM<sub>WT</sub>:TRPV5<sup>655-725</sup> complexes.** (A) <sup>15</sup>N-<sup>1</sup>H-HSQC spectra of CaM<sub>12</sub> upon addition of 0.0 (black), 1.0 (red), 2.0 (blue) molar equivalent of TRPV5<sup>655-725</sup>. Note that the blue 1:2 peaks are overlapping within the linewidth and hence near invisible; (B) <sup>15</sup>N-<sup>1</sup>H-HSQC spectra of CaM<sub>WT</sub> upon addition of TRPV5<sup>655-725</sup>, stoichiometries and color coding identical to (A); (C) <sup>1</sup>H-<sup>15</sup>N-CSP analysis of CaM<sub>12</sub> upon binding of TRPV5<sup>655-725</sup> (1:1 complex vs. unbound); (D) <sup>1</sup>H-<sup>15</sup>N-CSP analysis of CaM<sub>WT</sub> upon binding of TRPV5<sup>655-725</sup> (1:1 complex vs. unbound); (E) <sup>1</sup>H-<sup>15</sup>N-CSP analysis of CaM<sub>12</sub> upon binding of TRPV5<sup>655-725</sup> (1:2 complex vs. 1:1 complex); Note that the scale is 5 times smaller as compared to the scale of (F) and all effects fall within the margin of error; (F) <sup>1</sup>H-<sup>15</sup>N-CSP analysis of CaM<sub>WT</sub> upon binding of TRPV5<sup>655-725</sup> (1:2 complex vs. 1:1 complex).

domains. Analysis of the residue-specific chemical shift perturbations (CSP) ( $\delta_{\text{bound}} - \delta_{\text{free}}$ ) as a function of residue number demonstrates the lobe-specificity of CaM:TRPV5 interaction (Figs 2C-F). Upon addition of equimolar amount of TRPV5<sup>655-725</sup> to both CaM<sub>12</sub> and CaM<sub>wt</sub> the largest perturbations are observed for the C-lobe residues (Figs 2C,D), with negligible effects on the CaM<sub>12</sub> N-lobe and small,



1  
2  
3 but relevant perturbations for the CaM<sub>WT</sub> N-lobe. Remarkably, the magnitudes of the  
4 C-lobe perturbations are very similar for CaM<sub>12</sub> and CaM<sub>WT</sub>, with the very large  
5 shifts observed for residues Phe92, Ala128 and Met144, which are located in the  
6 hydrophobic binding-pocket of the CaM C-lobe<sup>51</sup>. In contrast, upon addition of an  
7 excess amount of TRPV5, an additional set of perturbations was observed only for  
8 the residues from the Ca<sup>2+</sup>-loaded N-lobe of CaM<sub>WT</sub>, with no observable effects for  
9 the N-lobe of CaM<sub>12</sub> (Figs 2E,F). These CSP data illustrate the asymmetry in the  
10 interaction of TRPV5 with the CaM N- and C-domains and provide strong evidence  
11 that the formation of the complex between the CaM C-lobe and TRPV5 C-terminus  
12 plays a central role in the TRPV5 inactivation mechanism.  
13  
14  
15  
16  
17  
18  
19  
20  
21

### 22 ***Structure of the CaM<sub>12</sub>:TRPV5<sup>655-725</sup> complex***

23  
24 We aimed to establish the atomic basis of the TRPV5-CaM interaction under  
25 low Ca<sup>2+</sup> conditions, and therefore set out to solve the structure of the  
26 CaM<sub>12</sub>:TRPV5<sup>655-725</sup> complex by high-resolution solution NMR spectroscopy. To  
27 assign the side-chain resonances, H(C)CH- and (H)CCH-TOCSY and <sup>13</sup>C-NOESY  
28 spectra were collected for the complex and analysed in combination. Resonance  
29 assignments were achieved for 95% of side-chain atoms from the CaM<sub>12</sub> moiety of  
30 the complex (Fig. S4A).  
31  
32  
33  
34  
35

36 In-silico order predictions for TRPV5 by the PONDR server<sup>52</sup> suggests that  
37 the TRPV5 cytoplasmic sequence is predominately intrinsically disordered, with  
38 only the TRPV5<sup>700-708</sup> region predicted to be  $\alpha$ -helical (Fig. S4B). Indeed, triple-  
39 resonance data recorded for <sup>13</sup>C/<sup>15</sup>N-labelled TRPV5<sup>655-725</sup> in complex with  
40 unlabelled CaM, yielded data indicative of wildly varying motional regimes often  
41 compromising spectral quality (not shown). However, by combining direct <sup>13</sup>C-  
42 detected and conventional heteronuclear methods for the CaM<sub>12</sub>:<sup>13</sup>C-<sup>15</sup>N-TRPV5<sup>655-  
43 725</sup> sample, 100% of backbone and 87% of side-chain resonances were assigned for  
44 the structured region. Overall, 52% of the backbone and 42% of the side-chain  
45 proton resonances were assigned for the full TPRV5 moiety of the complex.  
46  
47  
48  
49  
50  
51  
52  
53  
54  
55  
56  
57  
58

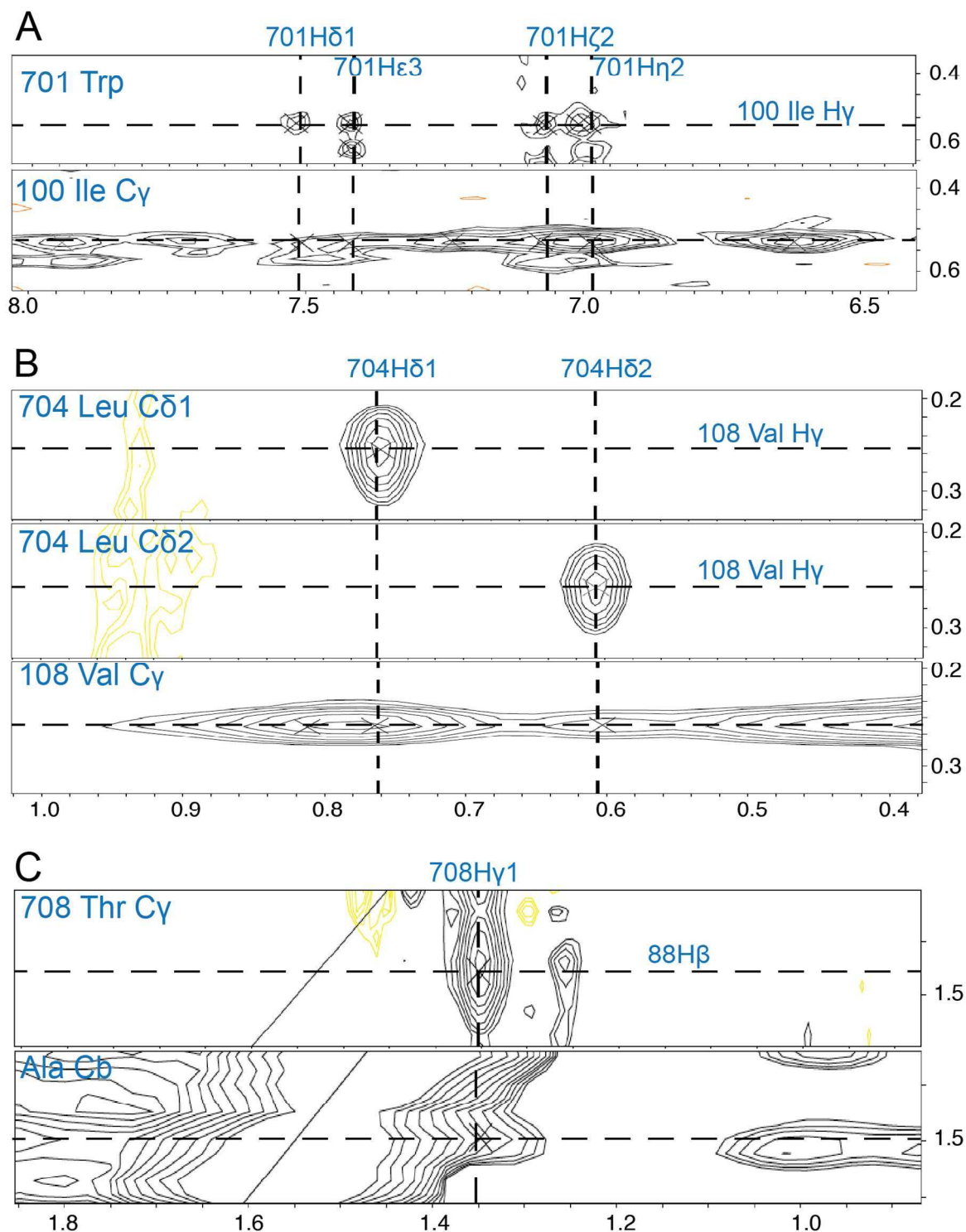


**Figure 3. Selected strips of  $^{13}\text{C}$ -NOESY spectra of the CaM $_{12}$ :TRPV $^{655-725}$  complex.** The strips display unambiguously assigned intermolecular NOEs between TRPV $^{655-725}$  and CaM $_{12}$ . (A) Matched strips showing the NOEs between the indole ring protons of Trp701 and the methyl groups of Ile100; (B) Matched strips showing the NOEs between the methyl groups of Leu704 and Val108; (C) Matched strips showing the NOEs between the methyl groups of Thr708 and Ala88. Horizontal dotted lines indicate proton assignments for the CaM $_{12}$  atoms, vertical dotted lines correspond to the assignments of the matching TRPV $^{655-725}$  protons, crosses indicate the centre of the peak.

1  
2  
3 In order to obtain the NOE distance restraints within and between the two  
4 chains of the complex, a series of 3D and 4D NOESY experiments (see Table S1)  
5 were collected and analysed for the different samples with different selectively  
6 isotope-labelled moieties of the complex. Individual NOE strips of 3D  $^{13}\text{C}$ -NOESY and  
7  $^{15}\text{N}$ -NOESY spectra, collected on the different samples, were manually inspected and  
8 cross-peaks consistent with intermolecular NOEs were identified. Interestingly, and  
9 in contrast to the expectations derived on the basis of the CaM-TRPV1 complex<sup>53</sup>,  
10 neither intermolecular NOEs between TRPV5<sup>655-725</sup> and the CaM N-lobe residues,  
11 nor long-range intermolecular NOEs between the CaM N- and C-lobes residues were  
12 observed, indicating the absence of any intramolecular contacts between the C- and  
13 N-lobes of CaM. In contrast, numerous intermolecular NOEs between the CaM C-lobe  
14 and the helical region of TRPV5<sup>655-725</sup> were identified in the  $^{13}\text{C}$ -NOESY spectra (Fig.  
15 3). The  $^{13}\text{C}$ -aromatic-NOESY spectrum displayed characteristic NOE cross peaks  
16 between Trp701 and the methyl groups of CaM<sub>12</sub> Ile100 (Fig. 3A). The symmetric  
17 NOE was also observed at the Ile100 C $\gamma$  strip in the  $^{13}\text{C}$ -NOESY-HSQC experiment  
18 (Fig. 3A), collected for the reciprocally labeled sample 1 (see Table S2.1). Similarly,  
19 NOEs were also observed between the TRPV5 Trp701 and other hydrophobic C-lobe  
20 residues, namely Ala128 and Met144. In accordance, these CaM<sub>12</sub> residues  
21 demonstrate the highest CSP values upon binding of TRPV5<sup>655-725</sup> (Fig. 2C). Trp701  
22 was previously identified as a key residue for the interaction<sup>13,54</sup>, and the  
23 observation of multiple intramolecular NOEs confirms that Trp701 anchors the  
24 TRPV5 C-terminal helix to the hydrophobic pocket of the CaM C-domain. Similarly,  
25 symmetric NOEs were also observed for Leu704, interacting with Phe92, Val108  
26 (Fig. 3B), Met109, and Phe141. In addition, intermolecular NOEs were found  
27 between the Methyl-protons of residues Ala88 and Val108 of CaM<sub>12</sub> and TRPV5  
28 residue Thr708, flanking the predicted helical region of TRPV5<sup>655-725</sup> (Fig. 3C).  
29  
30  
31  
32  
33  
34  
35  
36  
37  
38  
39  
40  
41  
42  
43  
44  
45  
46  
47  
48

49 The list of 16 upper limit restraints, derived from these unambiguously  
50 assigned intermolecular NOEs, together with a set of 268 dihedral angles restraints,  
51 generated using both TALOS+ and DANGLE software packages, and the otherwise  
52 unassigned NOESY peaklists were used in structure calculations, performed with  
53  
54  
55  
56  
57  
58

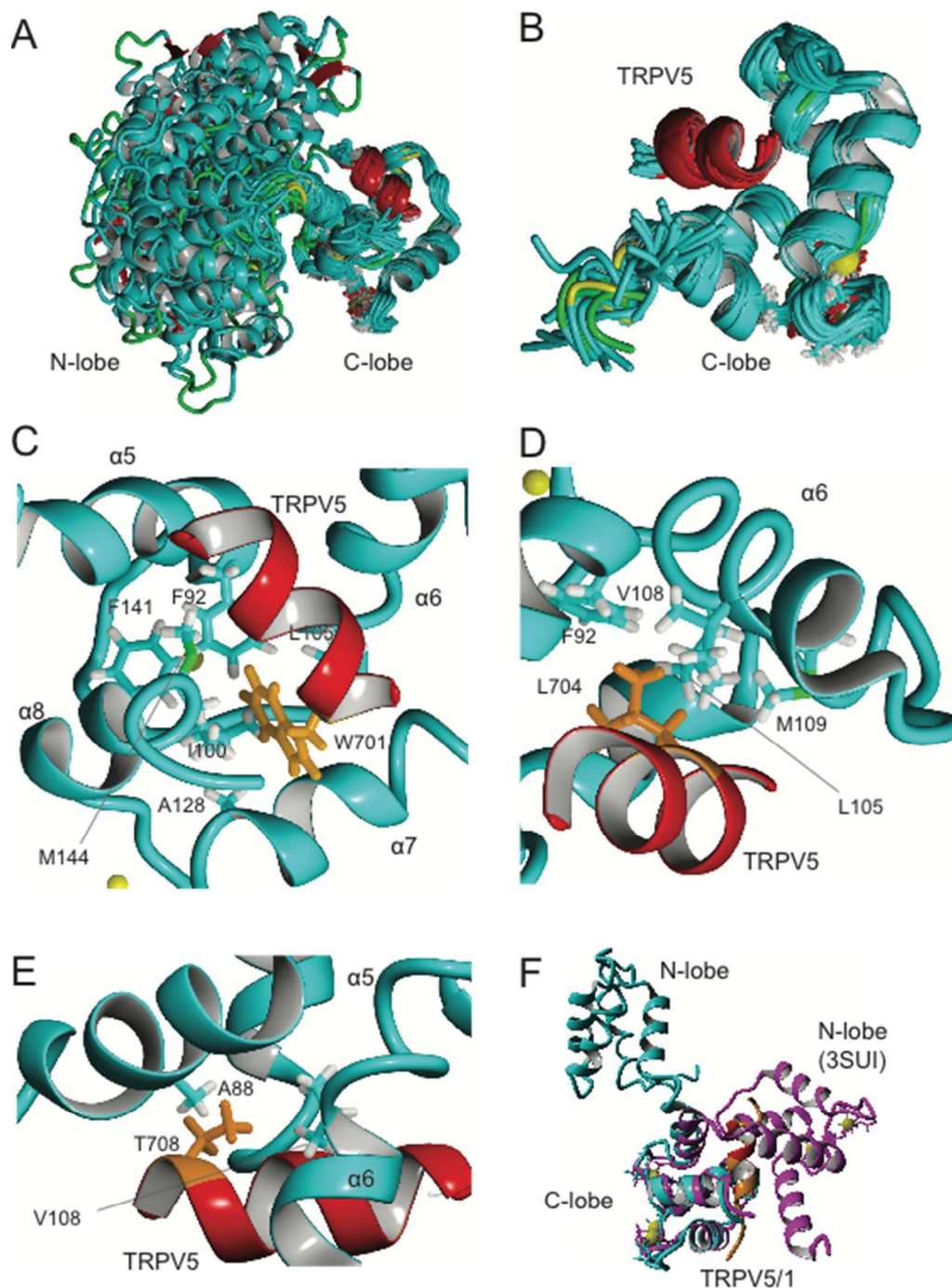


**Figure 4. Structure of the CaM<sub>12</sub>:TRPV5<sup>655-725</sup> complex.**

(A,B) CaM C-lobe and TRPV<sup>700-708</sup> best-fit backbone superposition of the 20 refined structures calculated for the complex, with N-lobe shown (A) and hidden (B). The TRPV<sup>700-709</sup> helix is colored red, CaM<sub>12</sub> is colored cyan; (C-E) Zoomed views, highlighting the surrounding side-chains of CaM<sub>12</sub> residues with detected NOE contacts as sticks, for Trp701, Leu704, and Thr708, respectively (orange); (F) Superimposed C-lobes of representative member of the CaM<sub>12</sub>:TRPV5<sup>655-725</sup> ensemble (cyan) and CaM in complex with the TRPV1 peptide (PDB id 3SUI; purple). The TRPV1 peptide (orange) and residues 700-709 of TRPV5 (red) are tightly overlapping.

1  
2  
3 CYANA/CANDID<sup>38</sup>. The program automatically generated 1804 unique NOE distance  
4 restraints from the available peaks (Table 1), with 119 of the 394 long-range NOEs  
5 identified as inter-chain NOEs. No inter-chain NOEs were observed for the residues  
6 located beyond the  $\alpha$ -helical region TRPV5<sup>700-708</sup> and the C-lobe region CaM<sub>12</sub><sup>74-148</sup>.  
7  
8  
9

10 Figure 4A shows the ensemble of the 20 lowest-energy structures calculated  
11 for the CaM<sub>12</sub>:TRPV5<sup>655-725</sup> complex after seven rounds of CYANA calculations  
12 followed by a water refinement protocol (see Methods) aligned on the C-lobe. These  
13 structures were assessed for the absence of upper distance NOE violations > 0.5 Å,  
14 and absence of dihedral angle violations > 5° after their initial CYANA calculations  
15 and demonstrated good convergence with an acceptable pairwise rmsd value of  
16 <1.2 Å for the backbone atoms in the regions CaM<sub>12</sub><sup>78-148</sup> and TRPV5<sup>700-708</sup> (see Table  
17 1 for structure calculation statistics). In accordance with the previously discussed  
18 NOE data, no contacts were found between the CaM<sub>12</sub> N-lobe and TRPV<sup>655-725</sup> or CaM  
19 C-lobe, resulting in adoption of scattered conformations of the N-lobe with respect  
20 to the C-lobe (Fig. 4A). Predictably, the absence of inter-molecular restraints  
21 between the N-lobe and TRPV5<sup>655-725</sup>, leads to significantly higher values of the  
22 pairwise mean square deviation in the ensemble for the CaM<sub>12</sub> N-lobe residues, with  
23 respect to the C-lobe residues (2.1 Å vs. 1.2 Å, respectively).  
24  
25  
26  
27  
28  
29  
30  
31  
32  
33  
34

35 The structure of the complex shows that CaM<sub>12</sub> interacts with TRPV<sup>655-725</sup>  
36 through its C-lobe in an anti-parallel mode, with TRPV residues Gly700-Leu709 in a  
37 helical conformation and a topology similar to those reported for other CaM  
38 complexes, such as those with the Munc peptide<sup>55</sup> or the HIV-1 Matrix protein<sup>56</sup>. The  
39 major stabilizing factor for the interaction between the CaM C-lobe and TRPV<sup>700-709</sup>  
40 is the deep anchoring of the Trp701 and Leu704 side chains into the C-terminal  
41 hydrophobic pocket of CaM (Figs 4C,D). In accordance with numerous NOE cross-  
42 peaks, the indole ring of the Trp701 is in close proximity to residues Phe92, Ile100,  
43 Leu105, Ala128, Phe141 and Met144 (Fig. 4C). The methyl groups of Leu704 in the  
44 centre of the helix interact with the side chains of CaM<sub>12</sub> residues Phe92, Leu105,  
45 Val108 and Met109. The third key residue Thr708, located at the C-terminal end of  
46 the structured TRPV5<sup>655-725</sup> region, is inserted deep into the hydrophobic cleft  
47 between the helices  $\alpha$ 5 and  $\alpha$ 6 of CaM<sub>12</sub>, where it contacts residues Ala88 and  
48  
49  
50  
51  
52  
53  
54  
55  
56  
57  
58

Val108 and thus, determines the orientation of the TRPV5 helix along the CaM<sub>12</sub> helix  $\alpha$ 5 (Fig. 4E). Interestingly, the side-chain of Arg705 is packed between the side-chains of residues Met144 and Met145.

Table 1. Structural statistics

**Completeness of resonance assignments**

Backbone	96% (CaM <sub>12</sub> ) 100 % (TRPV5 <sup>700-708</sup> )
Side chain	95% (CaM <sub>12</sub> ) 87% (TRPV5 <sup>700-708</sup> )
Aromatic	88% (CaM <sub>12</sub> ) 90% (TRPV5 <sup>700-708</sup> )
Stereospecific methyl	0%

**Conformationally restricting restraints**

Distance restraints	
Total	1803
Intraresidue (i = j)	578
Sequential ( i-j  = 1)	485
Medium range (1 <  i-j  < 5)	346
Long range ( i-j  ≥ 5)	394
Inter-monomer (between CaM <sub>12</sub> and TRPV5 <sup>655-725</sup> )	119
Dihedral angle restraints	268
Hydrogen-bond restraints	0
Disulfide restraints	0
Number of restraints per residue	8.24
Number of long-range restraints per residue	1.79

**Residual restraint violations**

Average number of distance violations per structure	
0.1–0.2 Å	40.65
0.2–0.5 Å	6.4
>0.5 Å	0.05 (max 0.5)
Average no. of dihedral angle violations per structure	
1–5°	3.75
>5°	1.3 (max 9.98°)

1  
2  
3  
4  
5  
6  
7  
8  
9  
10  
11  
12  
13  
14  
15  
16  
17  
18  
19  
20  
21  
22  
23  
24  
25  
26  
27  
28  
29  
30  
31  
32  
33  
34  
35  
36  
37  
38  
39  
40  
41  
42  
43  
44  
45  
46  
47  
48  
49  
50  
51  
52  
53  
54  
55  
56  
57  
58  
59  
60**Model quality**

RMSD backbone atoms (Å), residues 81-113, 117-146	1.15 ± 0.17
RMSD heavy atoms (Å), residues 81-113, 117-146	1.82 ± 0.19
RMSD backbone atoms (Å), residues 698-710	0.74 ± 0.20
RMSD heavy atoms (Å), residues 698-710	1.84 ± 0.34
RMSD backbone atoms (Å), residues 2-39, 43-77	2.08 ± 0.51
RMSD heavy atoms (Å), residues 2-39, 43-77	2.64 ± 0.51
RMSD bond lengths (Å)	0.035
RMSD bond angles (°)	0.497

**Ramachandran statistics res 1-148, 700-708**

Core (%)	96.7%
Allowed (%)	3.1%
Generous (%)	0.1%
Disallowed (%)	0.0%

**Global quality scores (raw/Z score)**

WHATIF summary for the residues 1-148, 700-708

## Structure Z-scores

1st generation packing quality	1.765 ± 0.706
2nd generation packing quality	4.507 ± 1.379
Ramachandran plot appearance	0.505 ± 0.324
Chi-1/Chi-2 rotamer normality	-0.084 ± 0.683
Backbone conformation	-0.787 ± 0.451

## RMS Z-scores

Bond lengths	1.218 ± 0.008
Bond angles	0.561 ± 0.008
Omega angle restraints	0.500 ± 0.038
Side chain planarity	0.956 ± 0.083
Improper dihedral distribution	0.811 ± 0.027
Inside/Outside distribution	1.000 ± 0.029

**Model contents**

Ordered residue range	1-148, 700-708
Total no. of residues	218

### ***Backbone dynamics of CaM:TRPV5<sup>655-725</sup>***

In order to study the dynamics of the CaM backbone in apo-state and in complex with TRPV5, we measured  $^{15}\text{N}$ - $T_1$ ,  $^{15}\text{N}$ - $T_2$  and  $^1\text{H}$ - $^{15}\text{N}$  heteronuclear NOE rates for the backbone amides for the native  $^{15}\text{N}$ -CaM<sub>WT</sub>, 1:1  $^{15}\text{N}$ -CaM<sub>12</sub>:TRPV5<sup>655-725</sup> and 1:1  $^{15}\text{N}$ -CaM<sub>WT</sub>:TRPV5<sup>655-725</sup> complexes. The sets of relaxation rates demonstrate significant differences between the three CaM species in the average values of the N- and C-lobes residues (See Fig. S5). Using the individual values of  $T_1$  and  $T_2$ , we calculated residue-specific local correlation times  $\tau_c(i)$  using the method suggested by Fushman et al.<sup>37</sup>. Fig. 5 displays histograms of these local  $\tau_c(i)$  values, grouped by the N- and C-lobes for the three proteins. The individual lobes of CaM<sub>WT</sub> are expected to display an independent dynamic behaviour as result of the flexible residues in the central helix<sup>57</sup>. Indeed, the local  $\tau_c$  values of each of the lobes of unbound CaM<sub>WT</sub> show a similar distribution around  $\sim 6.4$  ns compatible with a protein domain of  $\sim 70$  residues (Fig. 5A).

According to the structure and CSP data reported above, CaM<sub>12</sub> is engaged with TRPV5<sup>655-725</sup> using its C-lobe only. In agreement with this finding, its C-lobe  $\tau_c$  value distribution is shifted to  $\sim 9.8$  ns (Fig. 5B), arguably due to the increased mass and anisotropy, whereas the N-lobe shows a different and much smaller increase to  $\sim 8$  ns. Presumably, this increase from 6.4 ns is caused by the increased drag exerted by the C-lobe now bound to the extensive TRPV5<sup>655-725</sup> moiety. The results, however, clearly indicate an independent dynamical behaviour of the two lobes in agreement with the absence of domain tethering. In contrast, the 1:1 CaM<sub>WT</sub>:TRPV5<sup>655-725</sup> complex is expected to behave as one, tightly bound species and indeed, its N- and C-lobe  $\tau_c$  value distributions (Fig. 5C) are now both similar and higher when compared to either native CaM or the 1:1 CaM<sub>12</sub>:TRPV5<sup>655-725</sup> complex and correspond to the motion of a monomeric molecule with an effective mass of  $\sim 20$  kDa.

In order to assess the dynamics of the TRPV5 moiety of the complex with CaM<sub>12</sub>, we also measured the relaxation rates for the 1:1  $^{15}\text{N}$ -TRPV5<sup>655-725</sup>: $^{15}\text{N}$ -CaM<sub>12</sub> sample. For the fifteen distinct assigned amide nitrogen atoms of TRPV5<sup>655-725</sup>, the values of local correlation times were obtained (Fig. S5C). Noticeably, a distinct group of residues, either within the TRPV5 helix or predicted to be  $\alpha$ -helical (Q706,



N707, T708, L709, G710, L716 and N717), have an average  $\tau_c$  value of 9.8 ns, close to the average  $\tau_c$  values for CaM<sub>12</sub> C-lobe bound to TRPV5<sup>655-725</sup>. In contrast, residues from the regions predicted to be intrinsically disordered, exhibited a dramatic increase in their T<sub>2</sub> values, and hence a lower  $\tau_c$  values, demonstrating a high level of mobility in the C-terminal region of TRPV5.

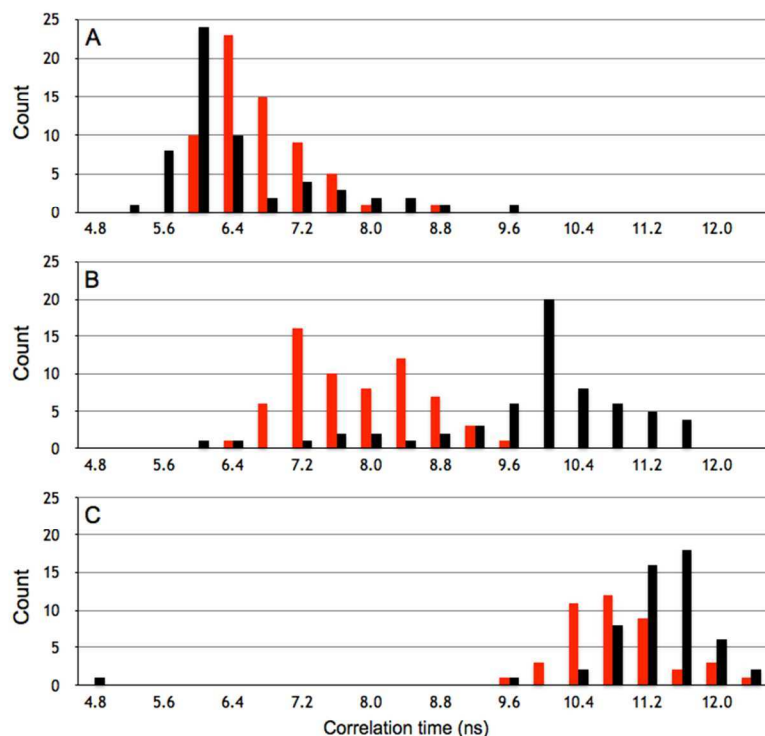


**Figure 5. Dynamics of free CaM and CaM:TRPV5<sup>655-725</sup> complexes.** Histograms of the distributions of the local correlation time values,  $\tau_c(i)$  for N-lobe residues (red) and C-lobe residues (black) for (A) free CaM<sub>WT</sub>, (B) 1:1 CaM<sub>12</sub>:TRPV5<sup>655-725</sup> and (C) 1:1 CaM<sub>WT</sub>:TRPV5<sup>655-725</sup>.

## Discussion

Our current study dissects the interaction between the TRPV5 C-terminus and CaM, thus identifying the tethering of CaM C-domain to TRPV5 monomer as a structural determinant of this interaction under low Ca<sup>2+</sup>-conditions. The interaction between either TRPV5, or the closely related TRPV6, and CaM has been

1  
2  
3 studied previously, both *in vitro* and in a cellular context<sup>11,13,54,58</sup>. Functionally  
4 similar CaM binding sites have also been identified in the vanilloid family members  
5 TRPV1<sup>59</sup> and TRPV4<sup>60</sup>, suggesting a common regulatory mechanism.  
6  
7

8  
9 In the recently published crystal structure of CaM in complex with the  
10 conserved C-terminal TRPV1 region, CaM forms a 1:1 complex with a canonical  
11 compact conformation, wrapping around the  $\alpha$ -helical TRPV1 C-terminus peptide  
12 using both N- and C-lobes<sup>53</sup>. Surprisingly, previous <sup>15</sup>N-HSQC analyses of the <sup>15</sup>N-  
13 CaM chemical shift differences upon titration with a short C-terminal TRPV5  
14 peptide, already revealed a non-canonical mode of interaction between the peptide  
15 and CaM, with an unusual 1:2 stoichiometry and more prominent effects observed  
16 for the CaM C-lobe<sup>3</sup>. These findings were also confirmed by ITC measurements and  
17 observed for the paralogue TRPV6<sup>27</sup>. In this current study we confirmed this  
18 unusual mode of interaction for longer TRPV5 fragments, alleviating the possibility  
19 that these effects originated from the insufficient length of the peptides. In contrast  
20 with the earlier TRPV5 work, however, we find that additional residues outside the  
21 previously defined minimal binding motif play an important role, affecting the  
22 patterns of interaction with CaM, as observed via NMR spectroscopy.  
23  
24  
25  
26  
27  
28  
29  
30  
31  
32

33 Our current studies also identify the tethering of the CaM C-lobe to the  
34 TRPV5 C-terminus as a crucial binding interaction. Indeed, the CSP values of the  
35 CaM C-lobe residues upon titration of TRPV5 are dramatically higher than those  
36 observed for the N-lobe residues and are nearly identical for both the wild-type CaM  
37 and the mutant CaM<sub>12</sub>. As the latter is unable to bind Ca<sup>2+</sup> by its N-lobe, we  
38 concluded that the CaM C-lobe, loaded with Ca<sup>2+</sup> even at basal intracellular Ca<sup>2+</sup>  
39 levels, mediates the interaction between TRPV5 and CaM (Fig 1, Fig. S2). Crucially,  
40 we established that <sup>1</sup>H-<sup>15</sup>N-NMR spectra of CaM purified under Ca<sup>2+</sup>-free conditions  
41 in complex with TRPV5<sup>655-725</sup> showed highly similar positioning of its C-lobe cross-  
42 peaks, indicative of the same structural arrangement as observed for the CaM<sub>WT</sub> and  
43 CaM<sub>12</sub> complexes, whereas most of its N-lobe cross-peaks were either shifted or  
44 even had disappeared altogether.  
45  
46  
47  
48  
49  
50  
51  
52  
53

54 To establish the molecular basis of the CaM<sub>12</sub>:TRPV5 complex, we solved its  
55 high-resolution solution structure and identified the key intermolecular interactions  
56  
57

1  
2  
3 that define the complex (Fig. 4). Our results show that CaM<sub>12</sub> interacts with a short  
4  $\alpha$ -helical region of TRPV5<sup>700-710</sup> exclusively by its C-lobe. The key hydrophobic  
5 TRPV5 residues Trp701, Leu704 and Thr708 are anchored in the hydrophobic  
6 pocket in the CaM C-lobe.  
7  
8  
9

10 Our structural findings are in agreement with a previous functional study,  
11 where the crucial role of Trp701, as well as Leu704, for CaM binding were  
12 demonstrated<sup>54</sup>. This study also reported that mutation of Arg705 led to diminished  
13 CaM binding and inhibited Ca<sup>2+</sup>-dependent inactivation of TRPV5. In our structure,  
14 the aliphatic part of the Arg705 side-chain is located in a groove between the side-  
15 chains of CaM<sub>12</sub> Met144 and Met145, which both demonstrate very large chemical  
16 shift changes upon TRPV5<sup>655-725</sup> binding. Our data suggest that it might be the  
17 binding affinity exerted by these Arg705-sidechain mediated interactions, rather  
18 than its charge, that are responsible for the effects of the mutation. Alternatively, an  
19 Arg705 mutation could affect the interactions with the N-lobe that ultimately result  
20 in formation of the 1:2 complex, crucial to the model of Bate et al.<sup>27</sup> (*vide infra*).  
21  
22  
23  
24  
25  
26  
27  
28  
29

30 Functional studies also showed that mutation of Thr708 to aspartate leads to  
31 diminished CaM binding and loss of Ca<sup>2+</sup>-induced CaM-dependent channel  
32 inactivation in HEK293 cells, and suggested that Thr708 is the target for  
33 parathyroid hormone-mediated phosphorylation of TRPV5<sup>12,54</sup>. Our structure  
34 suggests that phosphorylation of Thr708 would not need to abrogate binding to the  
35 CaM C-lobe. Indeed NMR titrations using peptides with either a phosphomimetic  
36 T708D mutation, or a phosphorylated T708 residue are capable of binding CaM<sub>WT</sub>  
37 (data not shown). As was the case for Arg705, we again speculate that N-lobe  
38 interaction required for 1:2 complex formation leading to channel inactivation may  
39 explain the *in vivo* observed effects.  
40  
41  
42  
43  
44  
45  
46

47 CaM displays a remarkable variability in its interactions with target  
48 sequences<sup>61</sup>. The positioning of the Trp-X-X-Leu-Arg-X-X-Thr CaM-C-lobe  
49 interacting residues in TRPV5 constitutes a short, high-affinity CaM-binding motif,  
50 which appears to be a shorter variation of the previously described 1-5-8-14 CaM-  
51 binding motif<sup>65</sup>. In the structure of the CaM<sub>12</sub>:TRPV5 complex, the 14<sup>th</sup> residue, i.e.  
52 Leu714, is clearly unstructured and does not display any interaction with the N-  
53  
54  
55  
56  
57  
58

1  
2  
3 lobe. It remains to be seen what role Leu714 would exert in the high-Ca<sup>2+</sup>  
4 CaM:TRPV5 complex. However, Leu712 would be most similar to the crucial TRPV6  
5 Leucine in the model of Bate et al.<sup>27</sup>.  
6  
7

8 The non-canonical Trp-X-X-Leu motif is also present in the solution  
9 structures of CaM in complex with a Munc1 peptide<sup>55</sup> and the HIV-1 Matrix  
10 protein<sup>56</sup>. Both these complexes adopt an extended conformation with a modular  
11 architecture where the N- and C-lobes of CaM interact with short, but distinct helical  
12 regions of the protein, linked by unstructured linker regions. C- or N-lobe only  
13 modes of interaction of CaM with a target peptide were also demonstrated for  
14 numerous other channels regulated by CaM, notably the voltage-gated Ca<sup>2+</sup>-  
15 channels<sup>62</sup>, voltage-gated Na<sup>+</sup>-channels<sup>63</sup>, small conductance calcium-activated  
16 potassium channels<sup>64</sup>, and aquaporins<sup>65</sup>.  
17  
18  
19  
20  
21  
22  
23

24 Our NMR relaxation studies of the unbound CaM<sub>wt</sub>, CaM<sub>wt</sub>:TRPV5<sup>655-725</sup> and  
25 CaM<sub>12</sub>:TRPV5<sup>655-725</sup> complexes showed independent dynamic behaviour of the two  
26 lobes for both these complexes and support the absence of domain tethering in the  
27 latter complex (Fig. 5). The increased correlation times for the CaM<sub>wt</sub>:TRPV5<sup>655-725</sup>  
28 complex, when compared to the unbound CaM<sub>wt</sub> and CaM<sub>12</sub>:TRPV5<sup>655-725</sup>, confirm  
29 the formation of a single complex for the wild-type, involving both lobes in the  
30 interaction.  
31  
32  
33  
34  
35  
36  
37

38 Altogether, our results establish a coordinating and crucial role of the CaM C-  
39 lobe in the formation of a high-affinity complex with the TRPV5 C-terminus under  
40 low-Ca<sup>2+</sup> conditions. It is tempting to speculate that CaM could be pre-bound to the  
41 TRPV5 intracellular C-terminus *in vivo* when the channel is an active state. At first  
42 glance, this idea appears to be in disagreement with a previous cellular study that  
43 implied a dynamic association between CaM and the related TRPV6 channel<sup>66</sup>.  
44 However, the latter study used a CaM<sub>1234</sub> mutant, defunct in Ca<sup>2+</sup> binding for both  
45 the N- and C-lobes, rather than the CaM<sub>12</sub> mutant used in our study. As also  
46 observed for the TRPV6 C-tail<sup>27</sup>, CaM<sub>1234</sub> abrogates all interaction with the TRPV5 C-  
47 tail as probed by our gel-filtration assays (Fig. S3). A pre-association between CaM  
48  
49  
50  
51  
52  
53  
54  
55  
56  
57  
58

1  
2  
3 and an intracellular channel terminus has previously also been postulated for the SK  
4 channels<sup>64</sup>, P/Q-type calcium channels<sup>67</sup> and voltage-gated sodium channels<sup>68</sup>.

6  
7 The TRPV5 C-tail is predicted and proven to be partially unstructured (Fig.  
8 S4) and the fragment used in this study is absent in the X-ray and EM structures of  
9 TRPV5, TRPV6, TRPV2 and TRPV1. We envision that the inherent flexibility is  
10 essential for the formation of the 1:2 CaM:TRPV5 complex as postulated by the  
11 model of Bate et al.<sup>27</sup>, where the bridging of two TRPV5 tails by CaM leads to  
12 channel inactivation. Interestingly, TRPV5 is capable of functioning as hetero-  
13 tetramer with TRPV6, suggesting that the C-tail behaviour should be similar. Indeed,  
14 TRPV6 has similarly unstructured regions and the 1-4-8 CaM C-lobe interaction  
15 motif is conserved between the two channels.  
16  
17  
18  
19  
20  
21  
22  
23

24 In conclusion, we propose our CaM<sub>12</sub>:TRPV5<sup>655-725</sup> structure as a  
25 representative for the low-calcium state of the novel three-state model for  
26 Ca<sup>2+</sup>/CaM-dependent inactivation of TRPV channels, as recently proposed by Bate et  
27 al.<sup>27</sup>. In accordance with this model, we postulate that Ca<sup>2+</sup> binding sites to the CaM  
28 N-lobe in response to elevated Ca<sup>2+</sup>-concentrations, effectively serves as the  
29 channel's Ca<sup>2+</sup> sensor. The Ca<sup>2+</sup>-loaded N-lobe can subsequently mediate the  
30 additional interactions, leading to engagement of the N-lobe across two channel tails  
31 and ultimately resulting in its inactivation.  
32  
33  
34  
35  
36  
37  
38  
39

#### 40 **Accession numbers**

41  
42 The chemical shifts and restraints were submitted to the BMRB (accession no.  
43 **34161**) and the ensemble of 20 conformers to the wwPDB (accession no. **5OEO**).  
44  
45  
46  
47  
48  
49  
50  
51  
52  
53  
54  
55  
56  
57  
58

## Acknowledgements

We thank Dr. Fred Muskett for expert support and maintenance of our NMR equipment. GWV acknowledges funding during various stages of this project by the Dutch Organization of Scientific Research (NWO; grants 700.55.443 and 700.57.101), BBSRC (grant BB/J007897/1) and MRC (grants MR/L000555/1 and MR/P00038X/1). We thank Dr. Skinner for his assistance with the initial setup of the CcpNmr Analysis CYANA pipeline. We thank Tessa Vuister for her help in editing and formatting of the manuscript.

## Supplementary materials

Five Figures and six Tables:  $^{15}\text{N}$ -HSQC spectra of short and long TRPV5 constructs;  $^{15}\text{N}$ -HSQC spectra of  $\text{CaM}_E$  and  $\text{CaM}_E:\text{TRPV5}$  complexes under varying conditions; Assignments and mobility plots;  $^{15}\text{N}$ -relaxation data of  $\text{CaM}$  and  $\text{TRPV5}^{655-725}$  as function of residue; gelshift essays assessing the binding of  $\text{CaM}_{WT}$ ,  $\text{CaM}_{1234}$ ,  $\text{CaM}_{12}$ , and  $\text{CaM}_{34}$  to the  $\text{TRPV5}^{655-725}$  fragment and six Tables with key experimental NMR parameters.

## References

- (1) van de Graaf, S. F. J., Hoenderop, J. G. J., Gkika, D., Lamers, D., Prenen, J., Rescher, U., Gerke, V., Staub, O., Nilius, B., and Bindels, R. J. M. (2003) Functional expression of the epithelial Ca<sup>2+</sup> channels (TRPV5 and TRPV6) requires association of the S100A10–annexin 2 complex. *EMBO J* 22, 1478–1487.
- (2) Frick, K. K., and Bushinsky, D. A. (2003) Molecular mechanisms of primary hypercalciuria. *J Am Soc Nephrol* 14, 1082–1095.
- (3) Hoenderop, J. G. J., van Leeuwen, J. P. T. M., van der Eerden, B. C. J., Kersten, F. F. J., van der Kemp, A. W. C. M., Mérillat, A.-M., Waarsing, J. H., Rossier, B. C., Vallon, V., Hummler, E., and Bindels, R. J. M. (2003) Renal Ca<sup>2+</sup> wasting, hyperabsorption, and reduced bone thickness in mice lacking TRPV5. *Journal of Clinical Investigation* 112, 1906–1914.
- (4) van Abel, M., Hoenderop, J. G. J., Dardenne, O., St Arnaud, R., van Os, C. H., van Leeuwen, H. J. P. T. M., and Bindels, R. J. M. (2002) 1,25-dihydroxyvitamin D(3)-independent stimulatory effect of estrogen on the expression of ECaC1 in the kidney. *J Am Soc Nephrol* 13, 2102–2109.
- (5) Chang, Q., Hoefs, S., van der Kemp, A. W., Topala, C. N., Bindels, R. J., and Hoenderop, J. G. J. (2005) The  $\beta$ -Glucuronidase Klotho Hydrolyzes and Activates the TRPV5 Channel. *Science* 310, 490–493.
- (6) Zhang, W., Na, T., and Peng, J.-B. (2009) Nedd4-2 and Nedd4 mediate degradation of TRPV6 and TRPV5. *The FASEB Journal* 23, 998.16–998.16.
- (7) Vennekens, R., Hoenderop, J., Prenen, J., Stuiver, M., Willems, P., Droogmans, G., Nilius, B., and Bindels, R. (2000) Permeation and gating properties of the novel epithelial Ca<sup>2+</sup> channel. *J Biol Chem* 275, 3963–3969.
- (8) Nilius, B., Prenen, J., Vennekens, R., Hoenderop, J. G. J., Bindels, R. J. M., and Droogmans, G. (2001) Modulation of the epithelial calcium channel, ECaC, by intracellular Ca<sup>2+</sup>. *Cell Calcium* 29, 417–428.
- (9) Lambers, T. T., Mahieu, F., Oancea, E., Hoofd, L., de Lange, F., Mensenkamp, A. R., Voets, T., Nilius, B., Clapham, D. E., Hoenderop, J. G. J., and Bindels, R. J. (2006) Calbindin-D-28K dynamically controls TRPV5-mediated Ca<sup>2+</sup> transport. *Embo Journal* 25, 2978–2988.
- (10) Gkika, D., Mahieu, F., Nilius, B., Hoenderop, J. G. J., and Bindels, R. J. M. (2004) 80K-H as a New Ca<sup>2+</sup> Sensor Regulating the Activity of the Epithelial Ca<sup>2+</sup> Channel Transient Receptor Potential Cation Channel V5 (TRPV5). *Journal of Biological Chemistry* 279, 26351–26357.
- (11) Lambers, T., Weidema, A., Nilius, B., Hoenderop, J. G. J., and Bindels, R. (2004) Regulation of the Mouse Epithelial Ca<sup>2+</sup> Channel TRPV6 by the Ca<sup>2+</sup>-sensor Calmodulin. *Journal of Biological Chemistry* 279, 28855.
- (12) de Groot, T., Lee, K., Langeslag, M., Xi, Q., Jalink, K., Bindels, R. J. M., and Hoenderop, J. G. J. (2009) Parathyroid hormone activates TRPV5 via PKA-dependent phosphorylation. *Journal of the American Society of Nephrology* 20, 1693–1704.
- (13) Kovalevskaya, N. V., Bokhovchuk, F. M., and Vuister, G. W. (2012) The TRPV5/6 calcium channels contain multiple calmodulin binding sites with differential binding properties. *J. Struct. Funct. Genomics* 13, 91–100.
- (14) Babu, Y. S., Sack, J. S., Greenhough, T. J., Bugg, C. E., Means, A. R., and Cook,

- 1  
2  
3 W. J. (1985) Three-dimensional structure of calmodulin. *Nature* 315, 37–40.
- 4 (15) Babu, Y. S., Bugg, C. E., and Cook, W. J. (1988) Structure of calmodulin refined at  
5 2.2 Å resolution. *J. Mol. Biol.* 204, 191–204.
- 6 (16) Nilius, B., Weidema, F., Prenen, J., Hoenderop, J. G. J., Vennekens, R., Hoefs, S.,  
7 Droogmans, G., and Bindels, R. J. (2003) The carboxyl terminus of the epithelial  
8 Ca<sup>2+</sup> channel ECaC1 is involved in Ca<sup>2+</sup>-dependent inactivation. *Pflugers Arch*  
9 445, 584–588.
- 10 (17) Cao, C., Zakharian, E., Borbiro, I., and Rohacs, T. (2013) Interplay between  
11 Calmodulin and Phosphatidylinositol 4,5-Bisphosphate in Ca<sup>2+</sup>-induced  
12 Inactivation of Transient Receptor Potential Vanilloid 6 Channels. *Journal of*  
13 *Biological Chemistry* 288, 5278–5290.
- 14 (18) Singh, B. B., Liu, X., Tang, J., Zhu, M. X., and Ambudkar, I. S. (2002) Calmodulin  
15 Regulates Ca<sup>2+</sup>-Dependent Feedback Inhibition of Store-Operated Ca<sup>2+</sup> Influx by  
16 Interaction with a Site in the C Terminus of TrpC1. *Mol Cell* 9, 739–750.
- 17 (19) Numazaki, M., Tominaga, T., Takeuchi, K., Murayama, N., Toyooka, H., and  
18 Tominaga, M. (2003) Structural determinant of TRPV1 desensitization interacts  
19 with calmodulin. *Proc. Natl. Acad. Sci. U.S.A.* 100, 8002–8006.
- 20 (20) Strotmann, R., Schultz, G., and Plant, T. D. (2003) Ca<sup>2+</sup>-dependent Potentiation of  
21 the Nonselective Cation Channel TRPV4 Is Mediated by a C-terminal Calmodulin  
22 Binding Site. *Journal of Biological Chemistry* 278, 26541–26549.
- 23 (21) Mercado, J., Gordon-Shaag, A., Zagotta, W. N., and Gordon, S. E. Ca<sup>2+</sup>-  
24 Dependent Desensitization of TRPV2 Channels Is Mediated by Hydrolysis of  
25 Phosphatidylinositol 4,5-Bisphosphate. *J. Neurosci.*  
26  
27 (22) Liao, M., Cao, E., Julius, D., and Cheng, Y. (2013) Structure of the TRPV1 ion  
28 channel determined by electron cryo-microscopy. *Nature* 504, 107–112.
- 29 (23) Zubcevic, L., Herzik, M. A., Chung, B. C., Liu, Z., Lander, G. C., and Lee, S.-Y.  
30 (2016) Cryo-electron microscopy structure of the TRPV2 ion channel. *Nat Struct*  
31 *Mol Biol* 23, 180–186.
- 32 (24) Hughes, T. E. T., Lodowski, D. T., Huynh, K. W., Yazici, A., Del Rosario, J.,  
33 Kapoor, A., Basak, S., Samanta, A., Han, X., Chakrapani, S., Zhou, Z. H., Filizola,  
34 M., Rohacs, T., Han, S., and Moiseenkova-Bell, V. Y. (2018) Structural basis of  
35 TRPV5 channel inhibition by econazole revealed by cryo-EM. *Nat Struct Mol Biol*  
36 1–12.
- 37 (25) Saotome, K., Singh, A. K., Yelshanskaya, M. V., and Sobolevsky, A. I. (2016)  
38 Crystal structure of the epithelial calcium channel TRPV6. *Nature* 534, 506–511.
- 39 (26) McGoldrick, L. L., Singh, A. K., Saotome, K., Yelshanskaya, M. V., Twomey, E.  
40 C., Grassucci, R. A., and Sobolevsky, A. I. (2018) Opening of the human epithelial  
41 calcium channel TRPV6. *Nature* 553, 233–237.
- 42 (27) Bate, N., Caves, R. E., Skinner, S. P., Goult, B. T., Basran, J., Mitcheson, J. S., and  
43 Vuister, G. W. (2018) A Novel Mechanism for Calmodulin Dependent Inactivation  
44 of Transient Receptor Potential Vanilloid 6. *Biochemistry* 57,  
45 DOI:10.1021/acs.biochem.7b01286.
- 46 (28) Wu, P.-R., Kuo, C.-C., Yet, S.-F., Liou, J.-Y., Wu, K. K., and Chen, P.-F. (2012)  
47 Lobe-Specific Calcium Binding in Calmodulin Regulates Endothelial Nitric Oxide  
48 Synthase Activation. *PLoS ONE* 7, e39851.
- 49 (29) Delaglio, F., Grzesiek, S., Vuister, G. W., Zhu, G., Pfeifer, J., and Bax, A. (1995)



- 1  
2  
3 NMRPipe: a multidimensional spectral processing system based on UNIX pipes. *J*  
4 *Biomol NMR* 6, 277–293.
- 5  
6 (30) Vranken, W. F., Boucher, W., Stevens, T. J., Fogh, R. H., Pajon, A., Llinás, M.,  
7 Ulrich, E. L., Markley, J. L., Ionides, J., and Laue, E. D. (2005) The CCPN data  
8 model for NMR spectroscopy: development of a software pipeline. *Proteins* 59,  
9 687–696.
- 10  
11 (31) Skinner, S. P., Fogh, R. H., Boucher, W., Ragan, T. J., Mureddu, L. G., and  
12 Vuister, G. W. (2016) CcpNmr AnalysisAssign: a flexible platform for integrated  
13 NMR analysis. *J Biomol NMR* 66, 111–124.
- 14  
15 (32) Hyberts, S. G., Milbradt, A. G., Wagner, A. B., Arthanari, H., and Wagner, G.  
16 (2012) Application of iterative soft thresholding for fast reconstruction of NMR  
17 data non-uniformly sampled with multidimensional Poisson Gap scheduling. *J*  
18 *Biomol NMR* 52, 315–327.
- 19  
20 (33) Bermel, W., Bertini, I., Duma, L., Felli, I. C., Emsley, L., Pierattelli, R., and Vasos,  
21 P. R. (2005) Complete assignment of heteronuclear protein resonances by  
22 protonless NMR spectroscopy. *Angew Chem Int Ed Engl* 44, 3089–3092.
- 23  
24 (34) Bermel, W., Bertini, I., Felli, I., Piccioli, M., and Pierattelli, R. (2006) <sup>13</sup>C-detected  
25 protonless NMR spectroscopy of proteins in solution. *Prog Nucl Mag Res Sp* 48,  
26 25–45.
- 27  
28 (35) Bax, A., Clore, G. M., and Gronenborn, A. M. (1990) <sup>1</sup>H-<sup>1</sup>H Correlation via  
29 Isotropic Mixing of <sup>13</sup>C Magnetization, a New Three-Dimensional Approach for  
30 Assigning <sup>1</sup>H and <sup>13</sup>C Spectra of <sup>13</sup>C-Enriched Proteins. *Journal of Magnetic*  
31 *Resonance* 88, 425–431.
- 32  
33 (36) Yamazaki, T., Forman-Kay, J. D., and Kay, L. E. (1993) Two-dimensional NMR  
34 experiments for correlating carbon-13.β. and proton.δ./ε. chemical  
35 shifts of aromatic residues in <sup>13</sup>C-labeled proteins via scalar couplings. *J Am Chem*  
36 *Soc* 115, 11054–11055.
- 37  
38 (37) Fushman, D., Weisemann, R., Thuring, H., and Rüterjans, H. (1994) Determination  
39 of the backbone mobility of ribonuclease T1 and its 2'GMP complex using  
40 molecular dynamics simulations and NMR relaxation data 4, 61–78.
- 41  
42 (38) Güntert, P. (2009) Automated structure determination from NMR spectra. *Eur*  
43 *Biophys J* 38, 129–143.
- 44  
45 (39) Skinner, S. P., Goult, B. T., Fogh, R. H., Boucher, W., Stevens, T. J., Laue, E. D.,  
46 and Vuister, G. W. (2015) Structure calculation, refinement and validation using  
47 CcpNmr Analysis. *Acta Crystallogr D Biol Crystallogr* 71, 154–161.
- 48  
49 (40) Shen, Y., Delaglio, F., Cornilescu, G., and Bax, A. (2009) TALOS+: a hybrid  
50 method for predicting protein backbone torsion angles from NMR chemical shifts.  
51 *J Biomol NMR* 44, 213–223.
- 52  
53 (41) Cheung, M.-S., Maguire, M. L., Stevens, T. J., and Broadhurst, R. W. (2010)  
54 DANGLE: A Bayesian inferential method for predicting protein backbone dihedral  
55 angles and secondary structure. *Journal of Magnetic Resonance* 202, 223–233.
- 56  
57 (42) Doreleijers, J. F., Sousa da Silva, A. W., Krieger, E., Nabuurs, S. B., Spronk, C. A.  
58 E. M., Stevens, T. J., Vranken, W. F., Vriend, G., and Vuister, G. W. (2012) CING:  
59 an integrated residue-based structure validation program suite. *J Biomol NMR* 54,  
60 267–283.
- (43) Krieger, E., and Vriend, G. (2014) YASARA View—molecular graphics for all

- 1  
2  
3 devices—from smartphones to workstations. *Bioinformatics* 30, 2981–2982.
- 4 (44) Bardiaux, B., Malliavin, T., and Nilges, M. (2012) ARIA for Solution and Solid-  
5 State NMR, in *Protein NMR Techniques*, pp 453–483. Humana Press, Totowa, NJ.
- 6 (45) Rieping, W., Habeck, M., and Nilges, M. (2005) Modeling errors in NOE data with  
7 a log-normal distribution improves the quality of NMR structures. *J Am Chem Soc*  
8 127, 16026–16027.
- 9  
10 (46) Montelione, G. T., Nilges, M., Bax, A., Güntert, P., Herrmann, T., Richardson, J.  
11 S., Schwieters, C. D., Vranken, W. F., Vuister, G. W., Wishart, D. S., Berman, H.  
12 M., Kleywegt, G. J., and Markley, J. L. (2013) Recommendations of the wwPDB  
13 NMR Validation Task Force. *Structure* 21, 1563–1570.
- 14 (47) Kovalevskaya, N. V., Schilderink, N., and Vuister, G. W. (2011) Expression and  
15 purification of the C-terminal fragments of TRPV5/6 channels. *Protein Expression*  
16 *and Purification* 80, 28–33.
- 17 (48) Linse, S., Helmersson, A., and Forsen, S. (1991) Calcium-Binding to Calmodulin  
18 and Its Globular Domains. *J Biol Chem* 266, 8050–8054.
- 19 (49) Bonventre, J. V., and Cheung, J. Y. (1986) Cytosolic Free Calcium-Concentration  
20 in Cultured Renal Epithelial-Cells. *American Journal of Physiology* 250, F329–  
21 F338.
- 22 (50) Gangola, P., and Rosen, B. P. (1987) Maintenance of Intracellular Calcium in  
23 *Escherichia Coli*. *J. Biol. Chem.* 262, 12570–12574.
- 24 (51) Ikura, M., Clore, G. M., Gronenborn, A., Zhu, G., Klee, C., and Bax, A. (1992)  
25 Solution structure of a calmodulin-target peptide complex by multidimensional  
26 NMR. *Science* 256, 632–638.
- 27 (52) Bin Xue, Dunbrack, R. L., Williams, R. W., Dunker, A. K., and Uversky, V. N.  
28 (2010) PONDR-FIT: A Meta-Predictor of Intrinsically Disordered Amino Acids.  
29 *Biochim Biophys Acta* 1804, 996–1010.
- 30 (53) Lau, S.-Y., Procko, E., and Gaudet, R. (2012) Distinct properties of Ca<sup>2+</sup>-  
31 calmodulin binding to N- and C-terminal regulatory regions of the TRPV1 channel.  
32 *J Gen Physiol* 140, 541–555.
- 33 (54) de Groot, T., Kovalevskaya, N. V., Verkaart, S., Schilderink, N., Felici, M., van der  
34 Hagen, E. A. E., Bindels, R. J. M., Vuister, G. W., and Hoenderop, J. G. (2011)  
35 Molecular Mechanisms of Calmodulin Action on TRPV5 and Modulation by  
36 Parathyroid Hormone. *Molecular and Cellular Biology* 31, 2845–2853.
- 37 (55) Rodriguez-Castañeda, F., Maestre-Martínez, M., Coudevylle, N., Dimova, K.,  
38 Junge, H., Lipstein, N., Lee, D., Becker, S., Brose, N., Jahn, O., Carlomagno, T.,  
39 and Griesinger, C. (2010) Modular architecture of Munc13/calmodulin complexes:  
40 dual regulation by Ca<sup>2+</sup> and possible function in short-term synaptic plasticity.  
41 *Embo Journal* 29, 680–691.
- 42 (56) Vlach, J., Samal, A. B., and Saad, J. S. (2014) Solution Structure of Calmodulin  
43 Bound to the Binding Domain of the HIV-1 Matrix Protein. *J Biol Chem* 289,  
44 8697–8705.
- 45 (57) Barbato, G., Ikura, M., Kay, L. E., Pastor, R. W., and Bax, A. (1992) Backbone  
46 dynamics of calmodulin studied by <sup>15</sup>N relaxation using inverse detected two-  
47 dimensional NMR spectroscopy: the central helix is flexible. *Biochemistry* 31,  
48 5269–5278.
- 49 (58) Niemeyer, B. A., Bergs, C., Wissenbach, U., Flockerzi, V., and Trost, C. (2001)

- 1  
2  
3 Competitive regulation of Ca<sup>T</sup>-like-mediated Ca<sup>2+</sup> entry by protein kinase C and  
4 calmodulin. *Proc Natl Acad Sci USA* 98, 3600–3605.
- 5 (59) Numazaki, M., Tominaga, T., Takeuchi, K., Murayama, N., Toyooka, H., and  
6 Tominaga, M. (2003) Structural determinant of TRPV1 desensitization interacts  
7 with calmodulin. *Proc Natl Acad Sci USA* 100, 8002–8006.
- 8 (60) Strotmann, R., Schultz, G., and Plant, T. D. (2003) Ca<sup>2+</sup>-dependent Potentiation of  
9 the Nonselective Cation Channel TRPV4 Is Mediated by a C-terminal Calmodulin  
10 Binding Site. *Journal of Biological Chemistry* 278, 26541–26549.
- 11 (61) Kovalevskaya, N. V., van de Waterbeemd, M., Bokhovchuk, F. M., Bate, N.,  
12 Bindels, R. J. M., Hoenderop, J. G. J., and Vuister, G. W. (2013) Structural analysis  
13 of calmodulin binding to ion channels demonstrates the role of its plasticity in  
14 regulation. *Pflugers Arch* 465, 1507–1519.
- 15 (62) Kim, E. Y., Rumpf, C. H., Fujiwara, Y., Cooley, E. S., Van Petegem, F., and  
16 Minor, D. L., Jr. (2008) Structures of CaV2 Ca<sup>2+</sup>/CaM-IQ Domain Complexes  
17 Reveal Binding Modes that Underlie Calcium-Dependent Inactivation and  
18 Facilitation. *Structure* 16, 1455–1467.
- 19 (63) Chagot, B., and Chazin, W. J. (2011) Solution NMR structure of Apo-calmodulin in  
20 complex with the IQ motif of human cardiac sodium channel NaV1.5. *J. Mol. Biol.*  
21 406, 106–119.
- 22 (64) Schumacher, M. A., Rivard, A. F., Bächinger, H. P., and Adelman, J. P. (2001)  
23 Structure of the gating domain of a Ca<sup>2+</sup>-activated K<sup>+</sup> channel  
24 complexed with Ca<sup>2+</sup>/calmodulin. *Nature* 410, 1120–1124.
- 25 (65) Reichow, S. L., and Gonen, T. (2008) Noncanonical binding of calmodulin to  
26 aquaporin-0: implications for channel regulation. *Structure* 16, 1389–1398.
- 27 (66) Derler, I., Hofbauer, M., Kahr, H., Fritsch, R., Muik, M., Kepplinger, K., Hack, M.  
28 E., Moritz, S., Schindl, R., Groschner, K., and Romanin, C. (2006) Dynamic but  
29 not constitutive association of calmodulin with rat TRPV6 channels enables fine  
30 tuning of Ca<sup>2+</sup>-dependent inactivation. *J Physiol (Lond)* 577, 31–44.
- 31 (67) Lee, A., Scheuer, T., and Catterall, W. A. (2000) Ca<sup>2+</sup>/calmodulin-dependent  
32 facilitation and inactivation of P/Q-type Ca<sup>2+</sup> channels. *J. Neurosci.* 20, 6830–  
33 6838.
- 34 (68) Sarhan, M. F., Tung, C.-C., Van Petegem, F., and Ahern, C. A. (2012)  
35 Crystallographic basis for calcium regulation of sodium channels. *Proc Natl Acad*  
36 *Sci USA* 109, 3558–3563.
- 37  
38  
39  
40  
41  
42  
43  
44  
45  
46  
47  
48  
49  
50  
51  
52  
53  
54  
55  
56  
57  
58

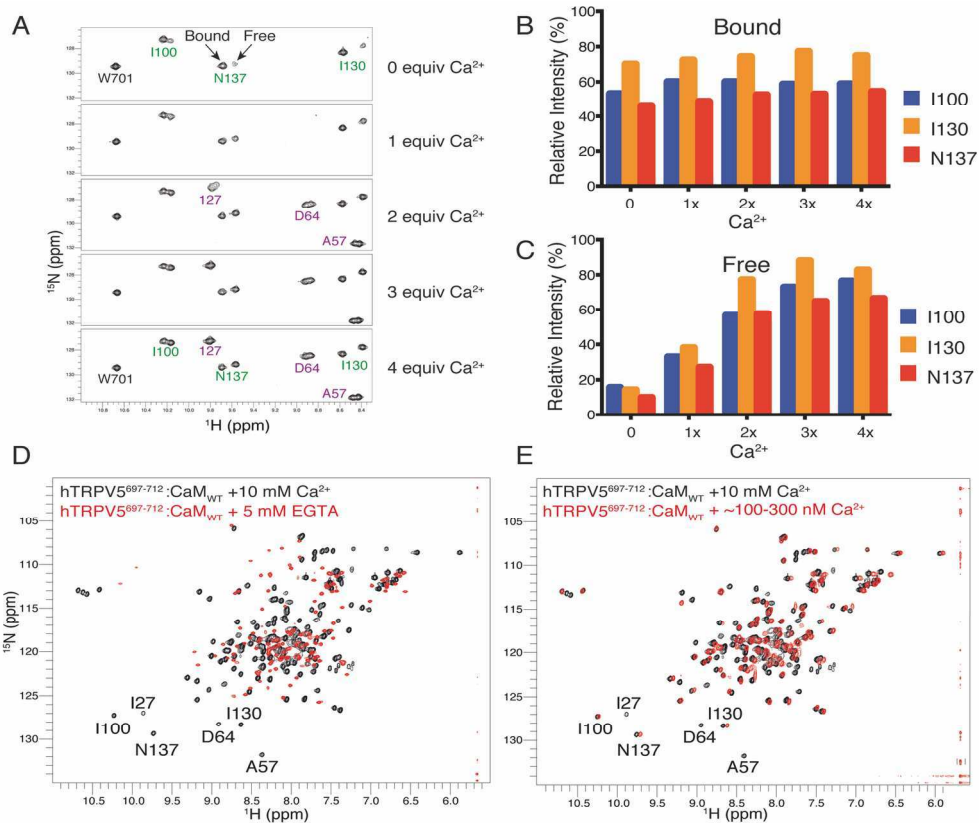
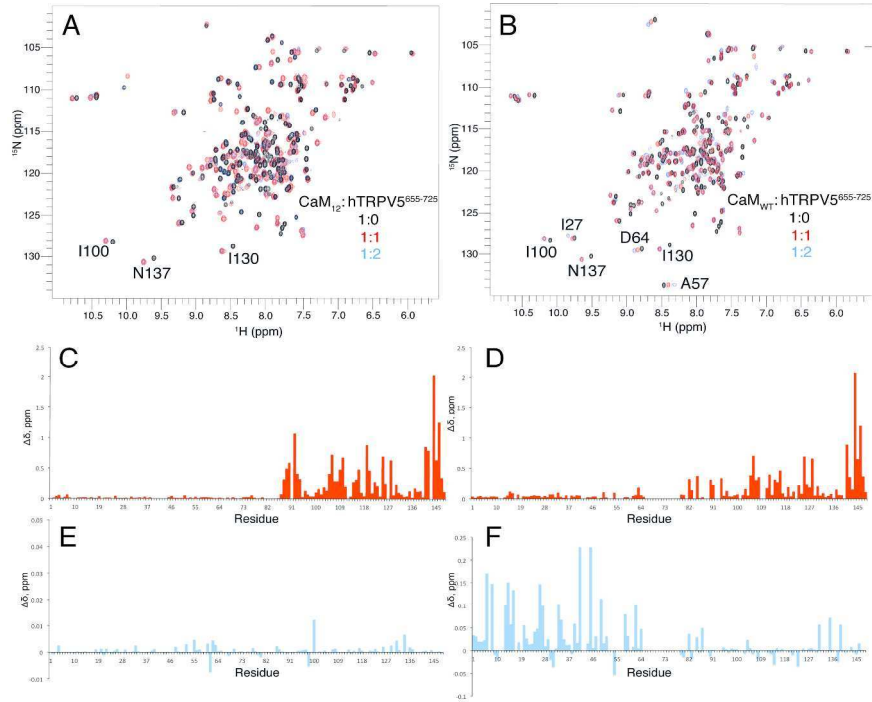
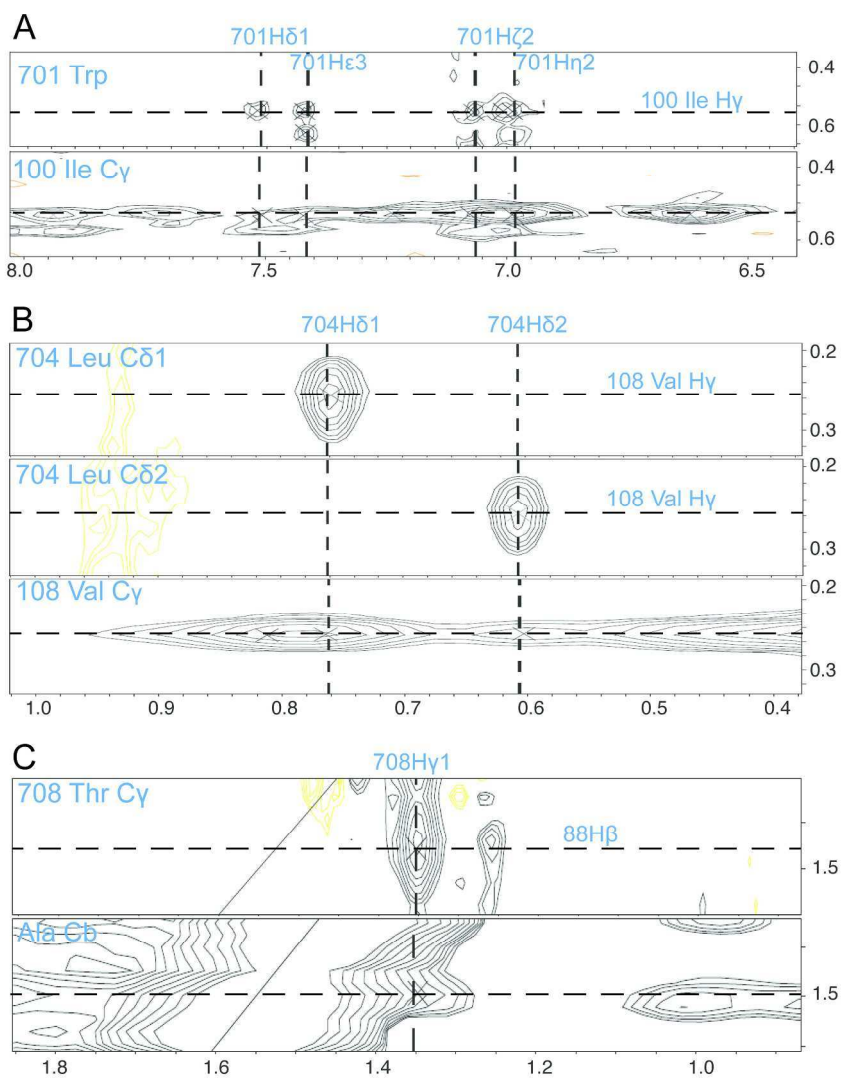


Figure 1

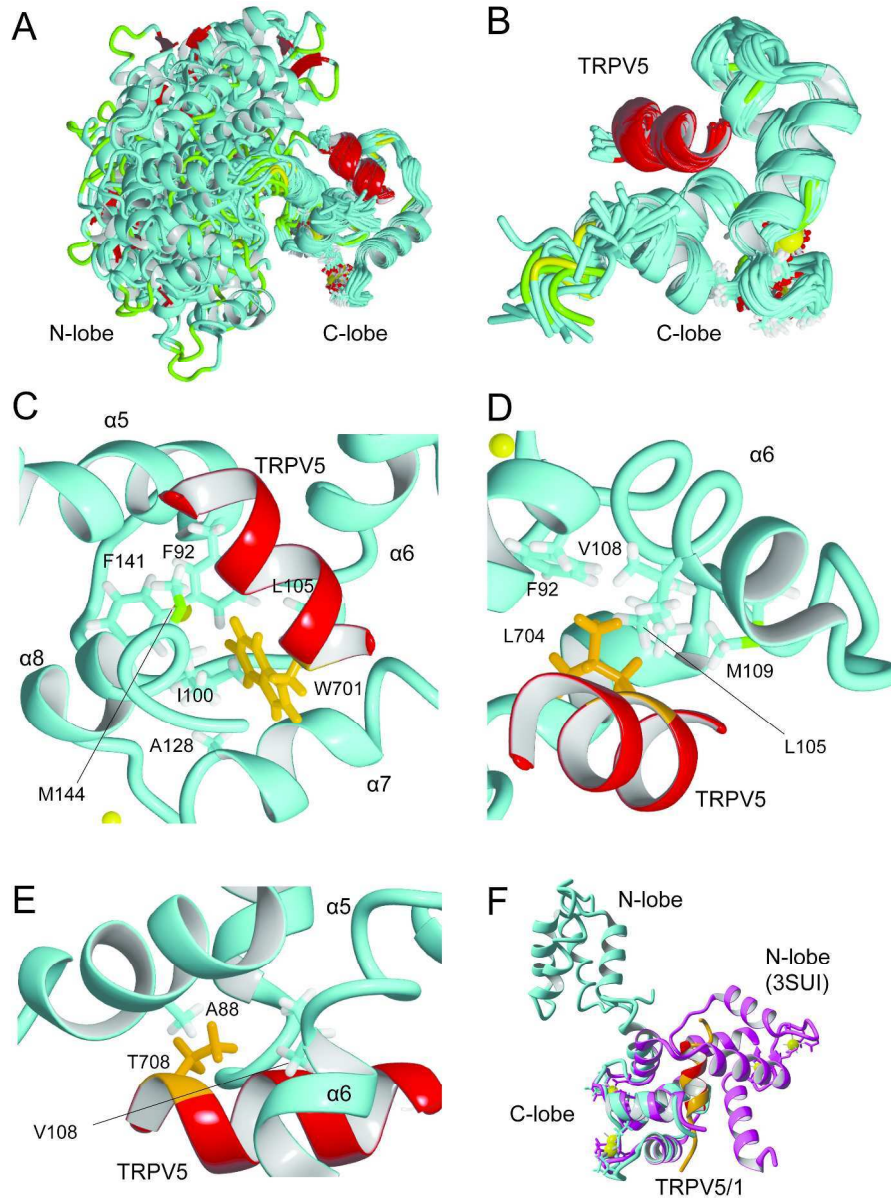
150x124mm (300 x 300 DPI)



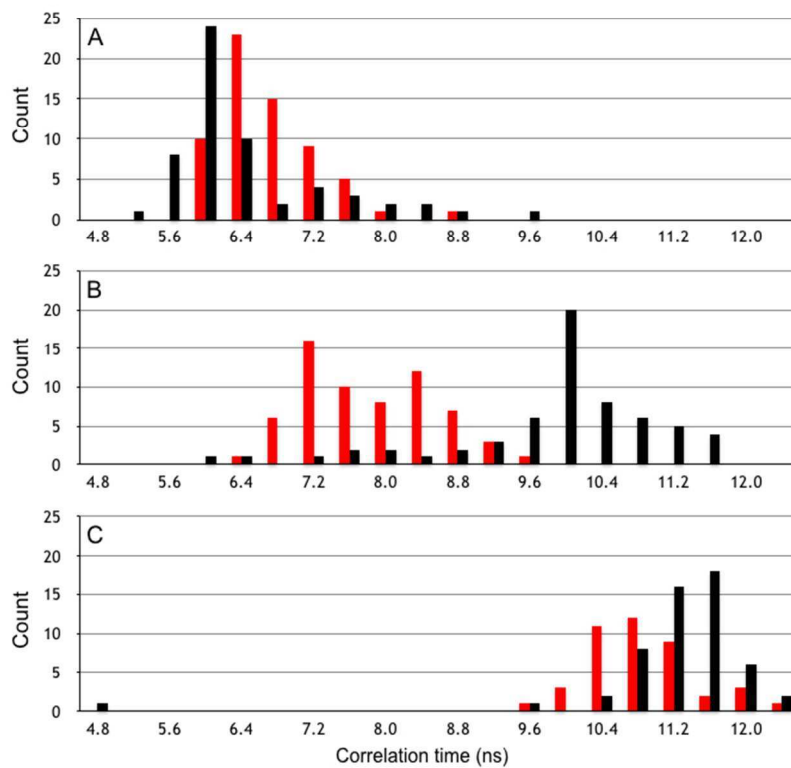
275x380mm (300 x 300 DPI)



221x285mm (300 x 300 DPI)



268x361mm (300 x 300 DPI)

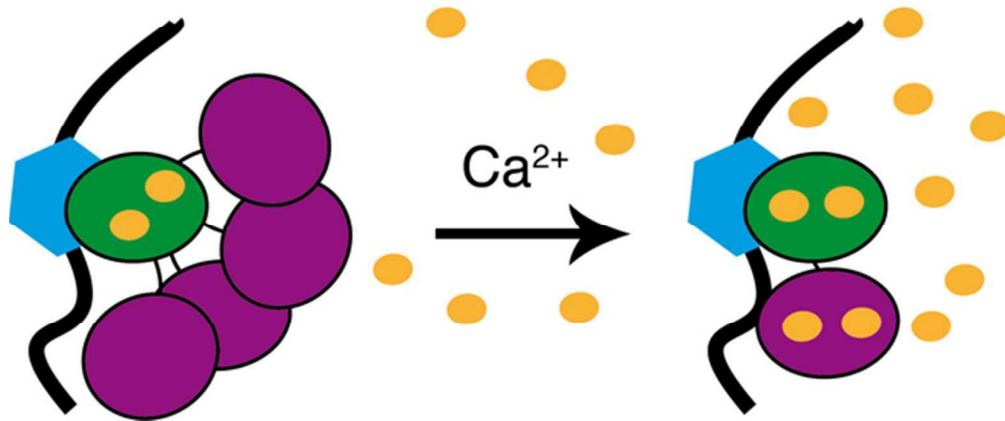


266x355mm (72 x 72 DPI)



1  
2  
3  
4  
5  
6  
7  
8  
9  
10  
11  
12  
13  
14  
15  
16  
17  
18  
19  
20  
21  
22  
23  
24  
25  
26  
27  
28  
29  
30  
31  
32  
33  
34  
35  
36  
37  
38  
39  
40  
41  
42  
43  
44  
45  
46  
47  
48  
49  
50  
51  
52  
53  
54  
55  
56  
57  
58  
59  
60

For Table of Contents use only



For Table of Contents only  
55x38mm (300 x 300 DPI)